Nordic Seas Acidification

Filippa Fransner[1], Friederike Fröb[2], Jerry Tjiputra[3], Melissa Chierici[4], Agneta Fransson[5],
Emil Jeansson[3], Truls Johannessen[1], Elizabeth Jones[4], Siv K. Lauvset[3], Sólveig R. Ólafsdóttir[6],
Abdirahman Omar[3], Ingunn Skjelvan[3], and Are Olsen[1]

[1]Geophysical Institute, University of Bergen, and Bjerknes Centre for Climate Research, Bergen, Norway
[2]Max Planck Institute for Meteorology, Hamburg, Germany
[3]NORCE Norwegian Research Centre, Bjerknes Centre for Climate Research, Bergen, Norway
[4]Institute of Marine Research, Fram Centre, Tromsø, Norway
[5] Norwegian Polar Institute, Tromsø, Norway
[6]Marine and Freshwater Research Institute, Reykjavík, Iceland

Correspondence: Filippa Fransner (filippa.fransner@uib.no)

Abstract. Being windows to the deep ocean, the Nordic Seas play an important role in transferring anthropogenic carbon, and thus ocean acidification, to the abyss. Due to its location in high latitudes, it is further more sensitive to acidification compared with many other oceanic regions. Here we make a detailed investigation of the acidification of the Nordic Seas, and its drivers, since pre-Industrial to 2100 by using in situ measurements, gridded climatological data, and simulations from one Earth System

5 Model (ESM). In the last 40 years, pH has decreased by 0.11 units in the Nordic Seas surface waters, a change that is twice as large as that between 1850-1980. We find that present trends are larger than expected from the increase in atmospheric CO_2 alone, which is related to a faster increase in the seawater pCO_2 compared with that of the atmosphere, i.e. a weakening of the pCO_2 undersaturation of the Nordic Seas. The pH drop, mainly driven by an uptake of anthropogenic CO_2, is significant all over the Nordic Seas, except for in the Barents Sea Opening, where it is counteracted by a significant increase in alkalinity.

10 We also find that the acidification signal penetrates relatively deep, in some regions down to 2000 meters. This has resulted in a significant decrease in the aragonite saturation state, which approaches undersaturation at 1000-2000 meters in the modern ocean. Future scenarios suggest an additional drop of 0.1-0.4 units, depending on the emission scenario, in surface pH until 2100. In the worst case scenario, RCP8.5, the entire water column will be undersaturated with respect to aragonite by the end of the century, threatening Nordic Seas cold-water corals and their ecosystems. The model simulations suggest that aragonite

15 undersaturation can be avoided at depths where the majority of the cold-water corals live in the RCP2.6 and RCP4.5 scenarios. As these results are based on one model only, we request additional observational and model studies to better quantify the transfer of anthropogenic CO_2 to deep waters and its effect on future pH in the Nordic Seas.

1 Introduction

Since 1750, human activities have released 675 ± 80 Gt of carbon to the atmosphere, of which 25% have been taken up by the oceans (Friedlingstein et al., 2019). Although the oceanic uptake of carbon dioxide (CO_2) mitigates immediate effects of global warming, it also has a more serious downside, namely a reduction of the seawater pH (e.g., Doney et al., 2009; Gattuso and Hansson, 2011). This ocean acidification imposes a serious threat to many marine organisms, in particular to those having shells and skeletons consisting of calcium carbonate, such as corals and pteropods (Doney et al., 2020; Doo et al., 2020). Since 1750, the global surface ocean pH has dropped by approximately 0.1 units (Doney et al., 2009; Gattuso and Hansson, 2011; Jiang et al., 2019). Future projections of surface ocean pH suggest a potential reduction of an additional 0.1-0.4 units until the end of the 21st century, depending on the CO_2 emission pathway (Bopp et al., 2013). While global average acidification, both from pre-Industrial times to present and that projected for the future is well constrained (Caldeira and Wickett, 2003; Raven et al., 2005; Kwiatkowski et al., 2020), less is known about its impacts on regional scales.

The Nordic Seas are of particular interest when it comes to ocean acidification. Being one of the few regions in the world ocean where deep water is formed (e.g. Våge et al., 2015; Chafik and Rossby, 2019), the Nordic Seas have a strong connection between surface and deep waters. As the northward flowing surface water, rich in anthropogenic carbon, is exported into the abyss and return southward following the Atlantic Meridional Overturning Circulation, the Nordic Seas would experience early and relatively large deep water acidification signals (Tjiputra et al., 2010; Perez et al., 2018). Furthermore, the Nordic Seas house cold-water coral reefs that are thought to be among the more vulnerable species to ocean acidification (Guinotte et al., 2006; Turley et al., 2007; Kutti et al., 2014). The already low saturation state of aragonite in the Nordic Seas (Ólafsson et al., 2009; Skjelvan et al., 2014), in combination with the strong connection between surface and deep waters, make these cold-water reefs particularly exposed to ocean acidification.

In this study we examine past, present and expected future ocean acidification rates and changes in aragonite saturation in the Nordic Seas, from surface to deep waters. We do so by using a combination of climatological distributions, modern observations, and Earth System Model (ESM) output. As the Nordic Seas is a dynamic region with a relatively short residence time of its surface waters, and where different water masses meet, its pH is also sensitive to other factors than anthropogenic carbon. To get a better understanding of how these other processes affects the acidification rates and their regional differences, we therefore separate the pH changes into their different drivers.

2 Drivers of pH change

Ocean acidification is defined as the drop in pH and calcium carbonate ($CaCO_3$) saturation state primarily caused by the oceanic uptake of anthropogenic CO_2, and the associated increase in seawater dissolved inorganic carbon (DIC) concentration. However, there are also other factors affecting the seawater pH. In order to understand the magnitude of the anthropogenic impact on seawater chemistry, it is therefore important to separate any observed change of pH into its different drivers. Apart from DIC concentration, seawater pH and $CaCO_3$ saturation state are also controlled by temperature, salinity, and alkalinity (ALK). The effects of an increase in each property (direction only) is shown in Table 1.

Table 1. Direction of effects of an increase in temperature, salinity, DIC and ALK on pH and CaCO$_3$ saturation states.

Driver	pH	CaCO$_3$ saturation
Temperature	-	+
Salinity	Minor	Minor
DIC	-	-
ALK	+	+

Temperature and salinity affect the pH by altering the dissociation constants and the partitioning of DIC between its different constituents; dissolved CO$_2$ (CO$_{2(aq)}$), carbonic acid (H$_2$CO$_3$), bicarbonate (HCO$_3^-$), and carbonate (CO$_3^{2-}$). The relation between DIC and ALK influences the pH by affecting the total number of free H$^+$ ions. It is important to keep in mind that changes in DIC concentration are not only a result of the uptake of excess atmospheric CO$_2$, but that they can also come as a result of changes in primary production, remineralization and mixing between water masses.

The sensitivity of pH and CaCO$_3$ saturation to uptake of anthropogenic CO$_2$ is dependent on the buffer capacity of the seawater, which is largely determined by the concentration of carbonate ions [CO$_3^{2-}$] (e.g. Sarmiento and Gruber, 2006; Orr, 2011). Once absorbed in water, CO$_2$ reacts to form carbonic acid (CO$_2$+ H$_2$O $\longrightarrow$ H$_2$CO$_3$), and then most of this is neutralised by the strongest base in seawater, carbonate ion (H$_2$CO$_3$+ CO$_3^{2-}$ $\longrightarrow$ 2HCO$_3^-$), which has been supplied to the ocean by the weathering of carbonate and igneous rocks (Urey reaction). In waters with a high concentration of CO$_3^{2-}$, a larger fraction of the absorbed CO$_2$ is converted to bicarbonate and less remains as dissolved CO$_2$, implying a smaller increase in the seawater pCO$_2$. These waters therefore have the capability of absorbing more CO$_2$ for any given increase in atmospheric pCO$_2$ (CO$_2$ partial pressure), which also implies a larger decline in CaCO$_3$ saturation state. The drop in pH, on the other hand, is larger in waters with lower CO$_3^{2-}$ concentration as they have less ability to neutralise the carbonic acid; their buffer capacity is lower.

3 Hydrographic setting

The Nordic Seas are comprised of the Greenland, Iceland and Norwegian seas, which are separated by deep submarine ridges (Figure 1, Hansen and Østerhus, 2000). The boundaries of the Nordic Seas are the Fram Strait in the north, the Barents Sea Opening to the northeast and the Greenland-Scotland Ridge in the south. The circulation pattern of the Nordic Seas (e.g. Blindheim and Østerhus, 2013; Våge et al., 2013) is characterised by the warm, saline Atlantic waters that flow northward as the Norwegian Atlantic Current in the east, and cold and fresh waters of Arctic origin flowing southward as the East Greenland Current in the west. In the Greenland and Iceland seas, deep and intermediate water masses are formed through deep mixing. These water masses ultimately overflow the Greenland-Scotland Ridge and feed into the North Atlantic Deep Water and, as such, help to sustain the lower limb of the Atlantic Meridional Overturning Circulation (AMOC, Dickson and Brown, 1994).
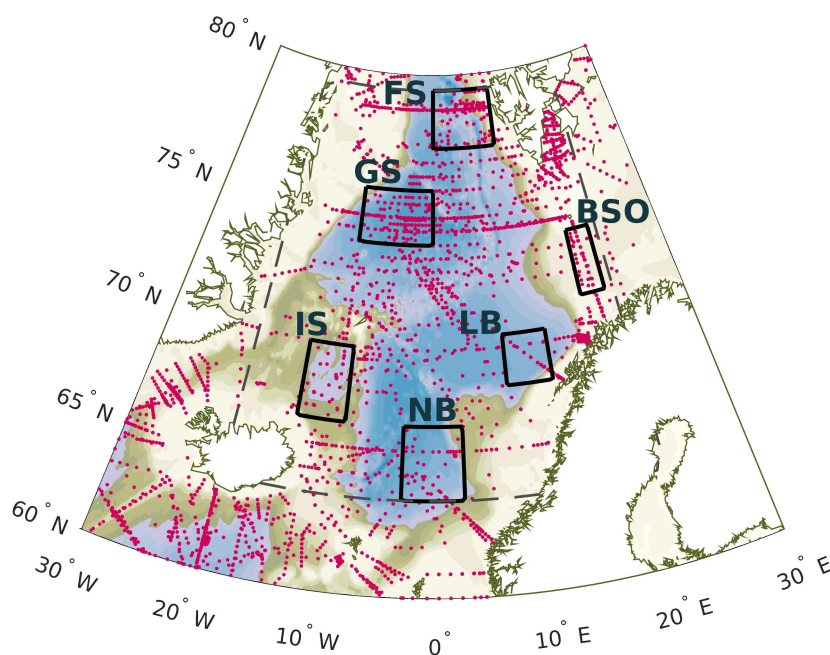
Figure 1. Map of the Nordic Seas with sampling locations (magenta). Also shown are the locations of the six regions where trends have been analyzed (rectangles); BSO: Barents Sea Opening; FS: eastern Fram Strait; GS: Greenland Sea; IS: Iceland Sea; LB: Lofoten Basin; NB: Norwegian Basin. The dashed gray line marks the area that we define as the Nordic Seas. The filled contours illustrate the bathymetry at 250 m intervals.

4 Data and methods

4.1 Observational data

This study makes use of DIC, ALK, temperature and salinity data collected between 1980 and 2019 during dedicated research cruises, at two time series stations, and in the framework of the Norwegian ocean acidification monitoring program. Sampling locations are shown in Fig. 1. Data from research cruises in the Nordic Seas were extracted from the GLODAPv2.2019 data product, which provides bias-corrected, cruise based, interior ocean data (Olsen et al., 2019). The GLODAPv2 data product is considered consistent to within 0.005 for salinity, 1 % for dissolved oxygen, 2 % for nitrate, 2 % for silicate , 2 % for phosphate, 4 μmol kg^{-1} for DIC and 4 μmol kg^{-1} for ALK (Olsen et al., 2019). The data from the Ocean Weather Station M in the Norwegian Sea located at 66 °N and 2 °E have been described in Skjelvan et al. (2008). At this station, sampling at 12 depth levels between surface and seabed (2100 m) was carried out each month between 2002 and 2009, and 4-6 times each year between 2010 and 2019. The time series station in the Iceland Sea, covering the period of 1985-2019, is situated at

68 °N and 12.67 °W. It is visited approximately 4 times a year and samples are taken at 10-20 depth levels between surface and seabed at about 1900 m. The data have been described in Ólafsson et al. (2009). The data from the Norwegian ocean acidification monitoring program covers the period 2011-2019 (2011-2012 Tilførselsprogrammet and 2013-2019 Havforsuringsprogrammet) and were collected at several repeated hydrographic sections off the coast of Norway (Chierici et al., 2012,

90   2013, 2014, 2015, 2016, 2017; Jones et al., 2018, 2019, 2020). Data for the eastern Fram Strait were collected on cruises with RV Helmer Hansen within the CarbonBridge project, and on cruises with RV Lance (Chierici et al., 2019b) organized by the Norwegian Polar Institute. Most samples (about 60% in total) from the datasets described above were collected during spring and summer (April-September). As described further down, we are working with annual means in this study. Variations in sampling frequency of different seasons can therefore introduce variability in the annual means of the uppermost layer, which

95   can bias the trend estimates. Unfortunately, there are not enough data to allow for deseasonalization in order to remove bias associated with the data paucity of undersampled months or seasons. For atmospheric CO_2, we used annual mean atmospheric CO_2 mole fraction (xCO_2) from the Mauna Loa updated records, downloaded from www.esrl.noaa.gov/gmd/ccgg/trends/ .

4.2   Model data

For the estimates of past and future ocean acidification under various climate scenarios, we used outputs prepared for the

100   Coupled Model Intercomparison Project Phase 5 (CMIP5, Taylor et al., 2012) and IPCC AR5 (IPCC, 2014), by the fully coupled Norwegian Earth System Model (NorESM1-ME, Bentsen et al., 2013; Tjiputra et al., 2013). NorESM1-ME includes the dynamical isopycnic vertical coordinate ocean model MICOM (Bleck and Smith, 1990) and the Hamburg Oceanic Carbon Cycle model (HAMOCC5, Maier-Reimer et al., 2005), adapted to the isopycnic ocean model framework. The HAMOCC5 model simulates lower trophic ecosystem processes up to the zooplankton level, including primary production, remineralization

105   and predation, and full water column inorganic carbon chemistry. The large-scale model performance has been evaluated in (Tjiputra et al., 2013), whereas ecosystem changes in the Nordic Seas discussed in (Skogen et al., 2018).

For the period 1850 to 2005, NorESM1-ME simulations were conducted using historical forcing, consisting of solar radiation, prescribed atmospheric CO_2 concentrations, and aerosols. The future scenarios, from 2006 to 2100, were conducted under Representative Concentration Pathways 2.6, 4.5 and 8.5 (RCP2.6, RCP4.5, and RCP8.5) associated with different rates

110   of atmospheric CO_2 increase. Under the high-CO_2 emission scenario (RCP8.5) the NorESM1-ME simulates similar evolution of surface ocean carbon chemistry in various regions of the world ocean, as other CMIP5 models (Tjiputra et al., 2014).

As shown in Fig. 2, the modelled pH (both absolute value and temporal change) are comparable to the observed values in the surface waters. The simulated acidification across most other depth levels also broadly agree with the estimates from observations. However, the model has a positive bias of pH in deep waters (not shown). For the analysis of past and future pH,

115   aragonite saturation state (Ω_{Ar}) and calcite saturation state (Ω_{Ca}) in the Nordic Seas, we therefore apply the modelled rates of change of these properties to the gridded GLODAPv2 climatology to calculate the past and future states. This is similar to procedures used by Orr et al. (2005) and Jiang et al. (2019). For the analysis of drivers of past and future acidification (Sect. 4.4), we additionally used the modelled temperature, salinity, DIC and ALK.

We decided to only use one ESM, as the rate of ocean acidification is a relatively straightforward process to model, and the
120 modelled rates of pH change have been shown to be comparable between CMIP-type ESMs (Bopp et al., 2013; Gehlen et al.,
2014; Kwiatkowski et al., 2020). The largest differences are normally found in deep waters, but the spread between models is
still smaller than the spread between scenarios.

4.3 Pre-industrial data

Apart from the pre-Industrial state estimate from NorESM1-ME, we also determined pre-Industrial pH and calcium carbonate
125 states by using the GLODAPv2 mapped climatology of pre-Industrial DIC (Lauvset et al., 2016). Because there are no estimates
of pre-Industrial temperature, salinity and ALK of the Nordic Seas, apart from ESM-simulations, we used the mapped present
day climatologies of these variables for the calculations. This only gives us the effect of the changing DIC on the pH since
pre-Industrial times.

4.4 Regional trends in pH and its drivers

130 Measurements of DIC, ALK, temperature, salinity and nutrients from the datasets described in Sect. 4.1 were used to calculate
pH, Ω_{Ar} and Ω_{Ca} using CO2SYS for MATLAB (Lewis and Wallace, 1998; van Heuven et al., 2011). For these calculations
we used the dissociation constants of Lueker et al. (2000), the bisulfate dissociation constant of Dickson (1990) and the borate-
to-salinity ratio of Uppström (1974). This ratio has recently been shown to be valid for the western Nordic Seas (Ólafsson
et al., 2020a). pH (on total scale), and the saturation states of aragonite (Ω_{Ar}) and calcite (Ω_{Ca}) where calculated using in situ
135 pressure and temperature.

Present trends in pH, Ω_{Ar} and Ω_{Ca} were determined for six different regions in the Nordic Seas representing different
hydrographic regimes. The six regions are: the Norwegian Basin (NB), the Lofoten Basin (LB), the Barents Sea Opening
(BSO), eastern Fram Strait (FS), the Greenland Sea (GS) and the Iceland Sea (IS). The geographical boundaries of each
of these are shown in Fig. 1. The Norwegian Basin, Lofoten Basin, and Barents Sea opening are all under the influence of
140 relatively warm and salty northward flowing Atlantic Water, while the Greenland and Iceland Seas are more influenced by
relatively cold and fresh southward flowing polar waters and are regions where deep convection occurs (e.g. Våge et al., 2015;
Brakstad et al., 2019). The Fram Strait is an area that is under influence of both Atlantic and polar waters. In order to minimize
the aliasing effects of latitudinal and longitudinal gradients, the north-south and east-west boundaries of each box were kept
as narrow as possible. For example, the boundaries of the Fram Strait box are constrained to the east, in order to ensure that
145 this mostly represents the influence of Atlantic Waters. Regional trends were computed for five different depth ranges (0-200,
200-500, 500-1000, 1000-2000, and 2000-4000 m). A thickness of 200 m was used for the surface layer since this sets the
approximate limit for the influence of seasonal variations associated with e.g. primary production (e.g. Skjelvan et al., 2008).
The trends were calculated by applying a linear regression over annual mean values in each box for the period 1981 to 2019.
The standard error of the slope is the error of the trend estimate.

150 For the calculation of the pH drivers from 1981-2019, the observed long-term changes in pH were decomposed into contri-
butions from changes in temperature (T), salinity (S), ALK and DIC. To determine the effect of each driver, we followed Zeebe

and Wolf-Gladrow (2001) and Lauvset et al. (2015). First, the effect of each of these processes on the CO_2 fugacity (fCO_2) is determined following Takahashi et al. (1993) and Metzl et al. (2010):

$$\frac{dfCO_2}{dt} = \frac{\delta fCO_2}{\delta T}\frac{dT}{dt} + \frac{\delta fCO_2}{\delta S}\frac{dS}{dt} + \frac{\delta fCO_2}{\delta DIC}\frac{dDIC}{dt} + \frac{\delta fCO_2}{\delta ALK}\frac{dALK}{dt} \qquad (1)$$

155   Eq. 1 can be written as:

$$\frac{dfCO_2}{dt} = \tau\langle fCO_2\rangle\frac{dT}{dt} + \eta\frac{\langle fCO_2\rangle}{\langle S\rangle}\frac{dS}{dt} + \gamma\frac{\langle fCO_2\rangle}{\langle DIC\rangle}\frac{dDIC}{dt} + \Gamma\frac{\langle fCO_2\rangle}{\langle ALK\rangle}\frac{dALK}{dt} \qquad (2)$$

where the brackets denote the annual mean of a property, and the various sensitivities are:

$$\tau = \delta fCO_2/\delta T/\langle fCO_2\rangle$$
160   $$\eta = \delta fCO_2/\delta S \times \langle S\rangle/\langle fCO_2\rangle$$
$$\gamma = \delta fCO_2/\delta DIC \times \langle DIC\rangle/\langle fCO_2\rangle$$
$$\Gamma = \delta fCO_2/\delta ALK \times \langle ALK\rangle/\langle fCO_2\rangle$$

Here, γ and Γ are the Revelle factors for DIC and ALK, respectively. While the value of τ was set to 0.0423 °C^{-1} from
165 Takahashi et al. (1993), we calculated the local values for η, γ and Γ. These and the temporal trends of T, S, DIC and ALK were estimated with the observational data from 1981 to 2019 for each region and depth level.

    Second, the magnitude of each fCO_2 driver is converted to units of pH (Lauvset et al., 2015) by using Henry's law ($[CO_2] = k_0 \times fCO_2$), the expression for $d[H+]/d[CO_2]$ (equation 1.5.87 Zeebe and Wolf-Gladrow, 2001) and by acknowledging that $dpH = -([H^+]ln(10))^{-1}d[H^+]$:

170   $$\frac{dpH}{dt} = -\frac{1}{ln(10)[H^+]}\frac{d[H^+]}{d[CO_2]}\frac{k_0 \times dfCO_2}{dt} \qquad (3)$$

    This procedure was also used for calculating the drivers of past (1850-1980) and future 2006-2100 pH changes, using temperature, salinity, ALK and DIC data from NorESM1-ME output.

    The pH change expected in seawater that perfectly tracks the atmospheric pCO_2 (pH_{perf}) was determined in CO2SYS using local temperature, salinity and ALK and their respective changes. Any deviation between observed pH change and pH_{perf} is
175 explained by changes in the air-sea pCO_2 difference.

5   Results

The evolution of the average pH in surface waters of the Nordic Seas from 1850 to 2100, as evident in observational data and model simulations, is shown in Fig. 2. The pre-Industrial estimate of the average Nordic Seas surface pH agrees well between
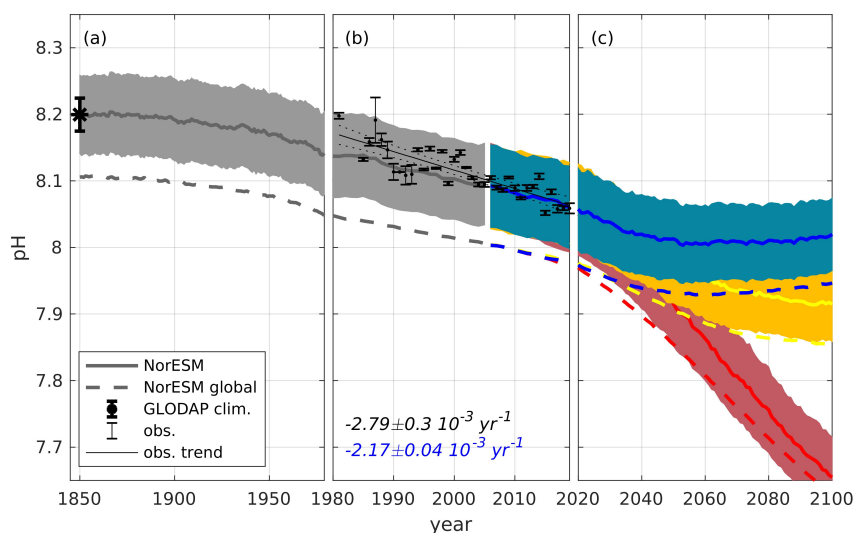
Figure 2. pH evolution, average over the Nordic Seas surface waters (0-200 m), from 1850 to 2100, separated into past (1850-1980), present (1981-2019) and future (2020-2100). Black dots with errorbars show the observed annual mean pH, with standard deviations, determined from all available observations in the Nordic Seas shown in Fig. 1, including those outside our regional boxes. The solid and dotted black lines show the trend calculated from the observations and its 95% confidence interval. The gray, red, yellow and blue solid lines show output from the NorESM1-ME historical and the RCP8.5, RCP4.5 and RCP2.6 future simulations, respectively, where the shading depicts the spatial variation (standard deviation). Note that this is the actual modelled data, and not the modelled rates of changes applied to observational data. The dashed lines show the evolution of global surface ocean pH from the same simulations. The black star (1850) with errorbars show an estimate of the pre-Industrial mean pH with standard deviation, derived from the GLODAPv2 mapped product as described in Sect. 4.3. The numbers in black and blue show the estimated trend with standard errors from the observations and the model, respectively, for the period of 1981-2019. Italics mean that the trend is significant.

GLODAPv2 and NorESM1-ME, with a mean value of 8.20±0.02 and 8.18±0.06, respectively. It is about 0.1 pH units higher
180   than the global average, which is related to the undersaturation of surface water in CO_2 in the Nordic Seas (Jiang et al., 2019). Our global average is lower than the one estimated by e.g. Jiang et al. (2019) for the surface ocean due to our 200 m thick surface layer. From 1850 to 1980, NorESM1-ME simulates a decline of about 0.05 pH units in the Nordic Seas and in the global ocean. For the period between 1981 and 2019, the modelled pH with standard deviations encompasses the observed one. The model and observations indicate an average decrease of surface pH of 0.08±0.00 and 0.11±0.01 units, respectively (Fig.
185   2). The trend estimated from the observations (-2.79±0.3 mpH yr^{-1}) is slightly stronger than the rate of decrease determined from model simulations (-2.17±0.04 mpH yr^{-1}), but there is more variability in the observations at the beginning of the period, which can impact the trend. The future evolution of surface water pH in the Nordic Seas depends strongly on the CO_2 emission scenario (Fig. 2). Under the high-CO_2 emission RCP8.5 scenario the pH is simulated to decrease by more than 0.4 units, to values below 7.7 by the end of the century. Also, the surface pH in the Nordic Seas and over the global ocean become more

190 similar with time in this scenario. This is due, partly to a modelled increase in the CO_2 undersaturation of the global ocean, and partly to a faster warming of high latitude oceans (not shown) probably related to Polar amplification (Dai et al., 2019). The RCP4.5 scenario, corresponding broadly to the CO_2 rise expected from currently pledged CO_2 emission reductions under the Paris agreement, results in a pH reduction half of that in RCP8.5. Until 2100, the surface pH is simulated to drop by about 0.2 units in this scenario, ending up at a value of 7.9. In the RCP2.6 scenario, where the CO_2 emissions are constrained to what

195 is needed to limit global warming to 2 °C, the pH stays at a value above 8 throughout the 21st century. It reaches its lowest value of slightly above 8 in the middle of the century, and then starts to increase again to reach a value of 8.02 by the end of the century. This passing decline is related to the overshoot profile of the radiative forcing, with a maximum atmospheric CO_2 of 443 ppm mid-century and assumptions about net negative emissions that brings atmospheric CO_2 down to its final 2100 level of 421 ppm (van Vuuren et al., 2011).

5.1 Present distribution of pH and CaCO$_3$ saturation states

In the upper waters of the Nordic Seas there are large gradients in temperature, salinity, DIC and ALK (Fig. S7a-e), which all influence the climatological distribution of pH, Ω_{Ar} and Ω_{Ca} (Figs. 3b,e,h). Temperature and ALK (which is largely governed by ocean salinity) decrease from south to north and east to west, from warm and saline Atlantic waters to colder and fresher polar waters. DIC increases from the warm waters of the south and east to the cold waters in the north and west, largely as a

205 consequence of the increased CO_2 solubility in colder water. However, as DIC also relates to salinity, low DIC waters are found on the east Greenland Shelf (e.g. Jeansson et al., 2011). The net effect of these drivers (Fig. 3b) is a southeast to northwest low to high gradient of pH, showing that temperature effects dominate. This dominates over the effect of the high DIC and low ALK concentrations in these waters, which would otherwise result in low pH. Along the Greenland coast, however, ALK and DIC effects dominate, resulting in relatively low pH. It is important to note that the GLODAPv2 climatology along the northern

210 Greenland coast is strongly influenced one cruise in 1993, and is therefore not representative for a long-term climatology.

In contrast to what might be expected from the higher pH in polar waters compared with waters of Atlantic origin, the Ω_{Ar} and Ω_{Ca} show an opposite pattern, and high to low gradient of CaCO$_3$ saturation state from south-east to north-west. This is related to the climatological distribution of CO_3^{2-} concentration, which broadly follows the temperature gradients in surface waters (e.g. Orr, 2011; Jiang et al., 2019). Due to the higher CO_2 solubility, colder waters have the capacity to absorb more CO_2

215 at a given atmospheric pCO$_2$, which consumes more CO_3^{2-}. Consequently, in the Nordic Seas the [CO_3^{2-}] is higher in Atlantic waters than in polar waters, resulting in higher Ω_{Ar} and Ω_{Ca}. Considering the higher CO_3^{2-} concentration, and therefore the higher buffer capacity of Atlantic Waters, we would expect these to experience larger drops in saturation states for a given increase in the atmospheric pCO$_2$. Polar waters, on the other hand, would experience larger drops in pH.

5.2 Changes from pre-Industrial to present

220 Maps of changes in surface pH, Ω_{Ar} and Ω_{Ca} from pre-Industrial to present, calculated from the gridded GLODAPv2 data and rates of change from the NorESM1-ME historical run, are shown in Fig. 3c,f and i. The change from pre-Industrial to present is rather uniform across the Nordic Seas for all variables; pH decrease about 0.1 while Ω_{Ar} and Ω_{Ca} decrease by 0.4 and 0.6,
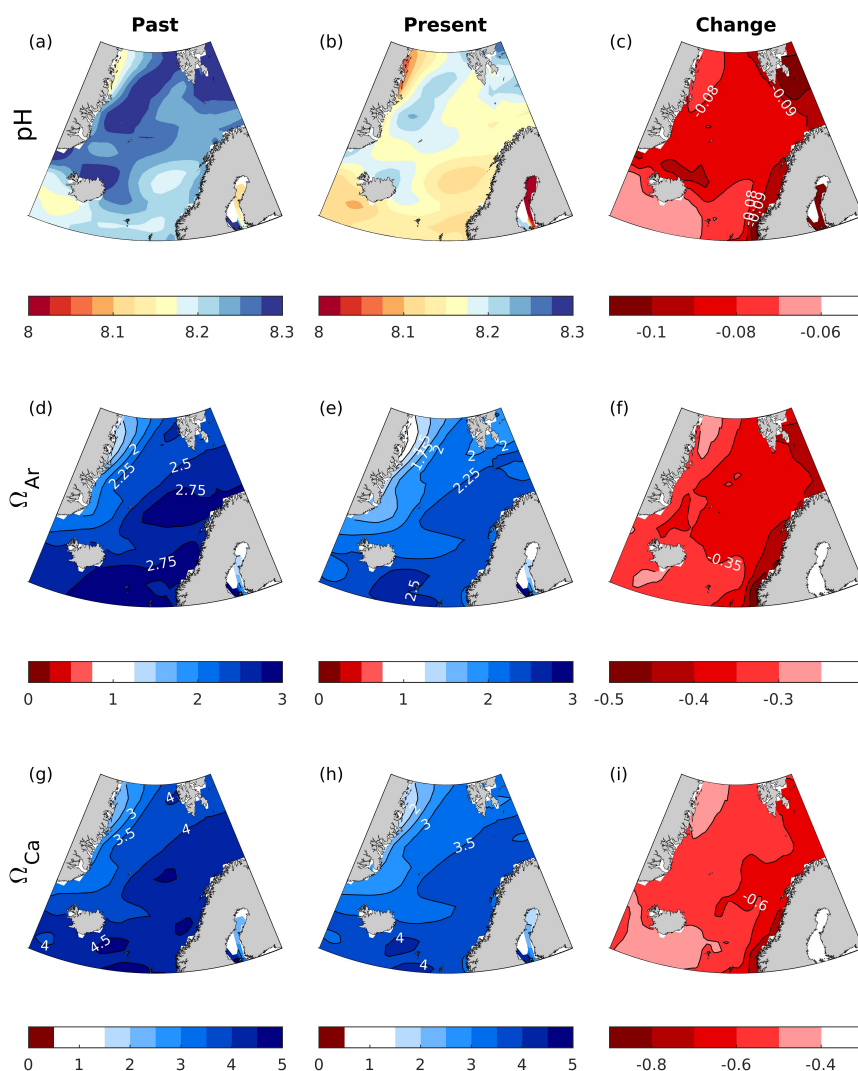
Figure 3. Maps of surface water pH, Ω_{Ar} and Ω_{Ca} for pre-Industrial (1850-1879) , present times (1980-2005), and the change in between the two periods. The maps were calculated from the GLODAPv2 gridded climatologies (Lauvset et al., 2016) as explained in Sect. 4.2 applying the simulated changes from past to present by NorESM1-ME.

respectively. In contrast to what is expected from the buffer capacity and the distribution of CO_3^{2-} ions as presented in Sect. 5.1, the pH decrease is slightly stronger in Atlantic waters than in polar waters. Over this period of time there is an overall

225   increase of the pCO$_2$ undersaturation of the Nordic Seas. The increase is weaker in Atlantic waters, meaning that there is a larger CO$_2$ uptake in these waters compared with polar waters, explaining the stronger reduction in pH. For Ω_{Ar} and Ω_{Ca}, there
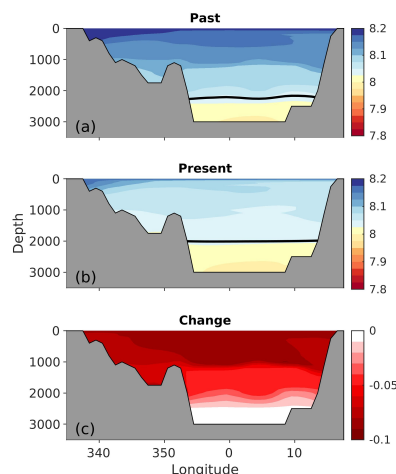
Figure 4. Zonal cross sections (at 70 °N) of pre-Industrial (1850-1879) and present pH (1980-2005), and the change between the two periods. The solid black line shows the saturation horizon of aragonite (Ω_{Ar}=1).

is a tendency of a stronger decrease in the Atlantic waters, as expected both from the CO_3^{2-} ion considerations summarized in Sect. 5.1, and also the larger decrease of Atlantic water pCO_2 undersaturation. Due to a gradually more limited connection with surface waters and the atmosphere, the impact of acidification decreases deeper into the water column. As shown in the
230   section across 70°N (Fig. 4), waters below 2500 m are nearly unaffected. While the entire water column remains saturated with respect to calcite, the saturation horizon (Ω=1) of aragonite shoaled slightly from pre-Industrial to present times, from a depth of 2200 m to a depth of 2000 m in this specific cross section. The mean displacement of the saturation horizon in the Nordic Seas will be shown in Sect. 6.2.

5.3   Present trends

235   Regional trends in observed ocean pH between 1981 and 2019 for the five different depth intervals considered are presented in Fig. 5. Due to the difference in sampled years between the basins, we cannot provide a robust comparison of the magnitude of trends between the basins. Nevertheless, we will here describe them in decreasing order. The largest decreases, of 2-3 mpH yr^{-1}, are found in surface waters (0-200 m). The uncertainties of these trends are approximately ±0.3-0.8 mpH yr^{-1}. An exceptionally strong reduction in surface pH (4 mpH yr^{-1}), but also with a large uncertainty (±1.46 mpH yr^{-1}) and a relatively
240   short sampling period, is found in the Lofoten Basin. Thereafter, the strongest significant trend is found in the Iceland Sea, followed by the Norwegian Basin, Fram Strait and the Greenland Sea. The weakest surface water trend occurred in the Barents Sea Opening, and is not significantly different from zero. The estimated trend in the Norwegian Basin of -2.73 ± 0.42 mpH yr^{-1} is significantly weaker than the -4.1 mpH yr^{-1} trend estimated for the period 1981-2013 by Skjelvan et al. (2014). This large difference in the Norwegian Basin can be a result of different sampling period, different definition of regions and potential
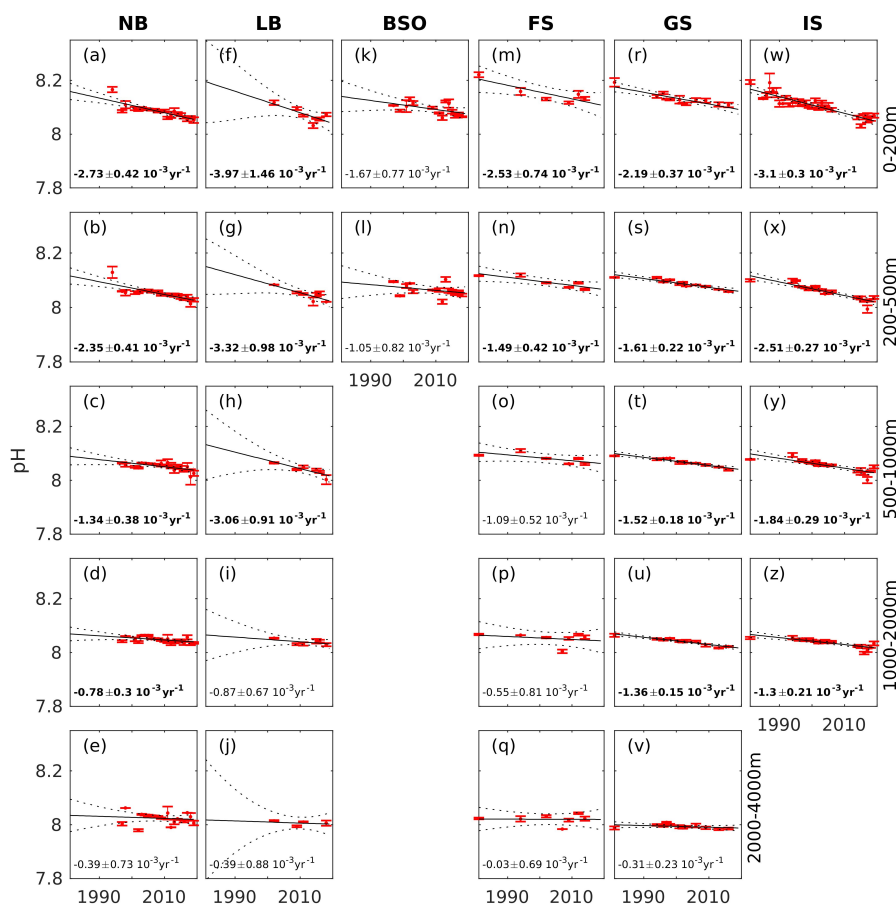
Figure 5. Estimated pH evolution from observational data in six different basins in the Nordic Seas at different depth intervals. Red dots with errorbars show annual means with standard deviations. The solid and dotted lines show the trend with 95% confidence intervals. The trend is indicated in the lower left of each panel. Bold indicates that the trend is significantly different from zero.

245   seasonal bias. However, our trend estimate in the Greenland Sea of -2.19 ± 0.37 mpH yr^{-1} agrees well with their trend of -2.3 mpH yr^{-1}.

     For deeper waters, the trends in pH are weaker compared with the 0-200 m layer, but remain relatively strong (decreasing by more than 2 mpH yr^{-1}) at the 200-500 m depth in the Norwegian Basin and the Iceland Sea. In the Fram Strait and the Greenland Sea the rate of change is around -1.5 mpH yr^{-1} at these depths. Only in the Barents Sea Opening the trend is weak 250   (1mpH yr^{-1}) and insignificant. In the Lofoten basin the trend stays around -3 mpH yr^{-1} down to 1000 m. At 500-1000 m, significant reductions in pH are also found in the Norwegian Basin, Greenland and Iceland Seas, between -2 and -1 mpH yr^{-1}. In the Fram Strait, there is no significant trend below 500 m. Only in the Greenland and the Iceland Seas the negative trend in pH stays relatively strong down to 2000 m, which could be a consequence of the stronger connection between deep and surface waters in these regions through deep winter mixing (Våge et al., 2015; Brakstad et al., 2019). However, the convection
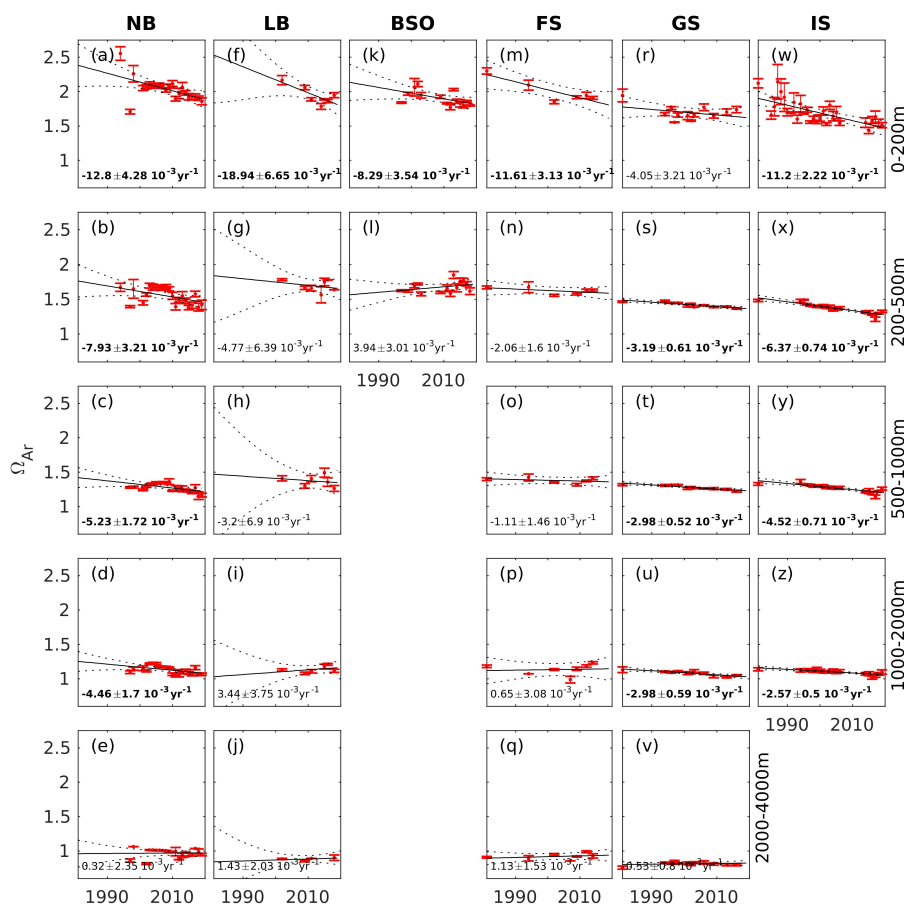
Figure 6. Estimated aragonite saturation state (Ω_{Ar}) evolution from observational data in six different basins in the Nordic Seas at different depth intervals. Red dots with errorbars show annual means with standard deviations. The solid and dotted lines show the trend with 95% confidence intervals. The trend is indicated in the lower left of each subplot. Bold indicates that the trend is significantly different from zero.

255   in the Iceland Sea has only been documented to reach depths of about 400 m (Ólafsson, 2003; Våge et al., 2015). The relatively strong signal in the deep Iceland Sea can therefore be a result of spreading of intermediate waters from the Greenland Sea (Messias et al., 2008; Jeansson et al., 2017). Also in the Norwegian Basin there is a significant trend down to 2000 m. It is weaker, but rather clear, and likely also a result of advection from the Greenland Sea (Blindheim, 1990; Blindheim and Rey, 2004; Jeansson et al., 2017). At 2000-4000 m, no significant change in pH can be detected. The water masses in this depth

260   range are increasingly dominated by old Arctic deep waters (e.g. Somavilla et al., 2013). With ages estimated to be around or more than 200 years (Jutterström and Jeansson, 2008; Stöven et al., 2016), they have been isolated from the anthropogenic CO_2 increase. Trends of aragonite and calcite saturation states are shown in Figs. 6 and S5, respectively. As for pH, the largest decreases are found in surface waters. For Ω_{Ar}, the rates of decline are in the order of 10^{-2} yr^{-1} and significant in all regions except for the Greenland Sea, where the decline is smaller, in the order of 10^{-3} yr^{-1}, and not significant. This relatively weak

265 decline in the Greenland Sea compared with the other regions is a result of the smaller decrease in DIC in combination with relatively strong increases in ALK and temperature, which counteracts the effect of acidification on the saturation states (while the temperature increase amplifies pH declines, see Sect. 6.1). Below 200 m, a significant reduction in Ω_{Ar} is found down to 2000 m in the Norwegian Basin and the Greenland and Iceland Seas. In the other regions no significant trends occurs below the surface layer. The waters in the depth range 1000-2000 m have gotten close to the limit of undersaturation of aragonite

270 during this period of time. Only the waters between 2000-4000 m, that are already undersaturated in aragonite, are more or less unaffected.

5.4   Future scenarios

In previous sections we have seen that the surface pH of the Nordic Seas, as for the global oceans, has decreased by more than 0.1 units on average since pre-Industrial times. The location of the saturation horizon of aragonite has displayed little change,

275 but the waters between 1000 and 2000 m are now close to undersaturated. The future evolution of pH in the Nordic Seas largely depends on how we regulate the emissions of anthropogenic CO_2 to the atmosphere (Fig. 2). Here we will present more details about the high and low-emission CMIP5 scenarios, RCP2.6 and RCP8.5, respectively, as simulated by NorESM1-ME.

In RCP2.6, the surface pH reaches its lowest value of 8.00 around 2050, and then starts to increase again to reach a value of 8.02 by the end of the century. Compared with present, an additional decline of 0.09-0.13 units in the surface waters is simulated

280 (Fig. 7c). The largest decreases are found in polar waters, leading to a weakening of the zonal gradient in pH that we see in the present and pre-Industrial climates. The surface Ω_{Ar} and Ω_{Ca} decrease by about 0.2-0.4 and 0.4-0.7 units, respectively. As for pH, the largest reductions are found in polar waters. Surface aragonite undersaturation is only expected for a small region of the northeastern Greenland shelf. The regional differences are explained by a larger increase of seawater pCO_2 in polar waters compared with Atlantic waters (not shown). Interestingly, the waters at 1000-2000 m depth experience a stronger decrease in

285 pH than surface waters in this scenario, which leads to a shoaling of the aragonite saturation horizon to a depth of 1000 m (Fig. 8). This layer of low pH water stretches over the entire basin, and is discussed in more detail in Sect. 6.1.

Under the RCP8.5 scenario, the pH in surface waters drops by about 0.4-0.5 units from present to a value of 7.7-7.8 in 2100 (Figs. 2 and 9). As for RCP2.6, the largest decrease takes place in polar waters. The change in this scenario is so strong that these waters becomes less basic than Atlantic waters, reversing the zonal pH gradient found in the pre-Industrial and present

290 climates. The surface Ω_{Ar} and Ω_{Ca} drop by around 1.0-1.1 and 1.6-1.8 units, respectively, with the largest declines taking place in the Atlantic Water. The pH drop under RCP8.5, is weaker in deeper than surface waters, as expected (Fig. 10). In contrast to present and pre-Industrial climates, the pH depth dependency is reversed; by the end of the century pH increases from the surface to deep ocean, reflecting that the input of anthropogenic carbon at the surface overrides the effect of remineralization in deep waters on the vertical pH gradient. The change in pH is large enough to make the entire water column, and consequently

295 also the seafloor, undersaturated in aragonite, the only exception being a thin surface layer in the Atlantic Water, possibly related to seasonal CO_2 drawdown. Ω_{Ca} also reaches low values, leading to undersaturation in polar waters.
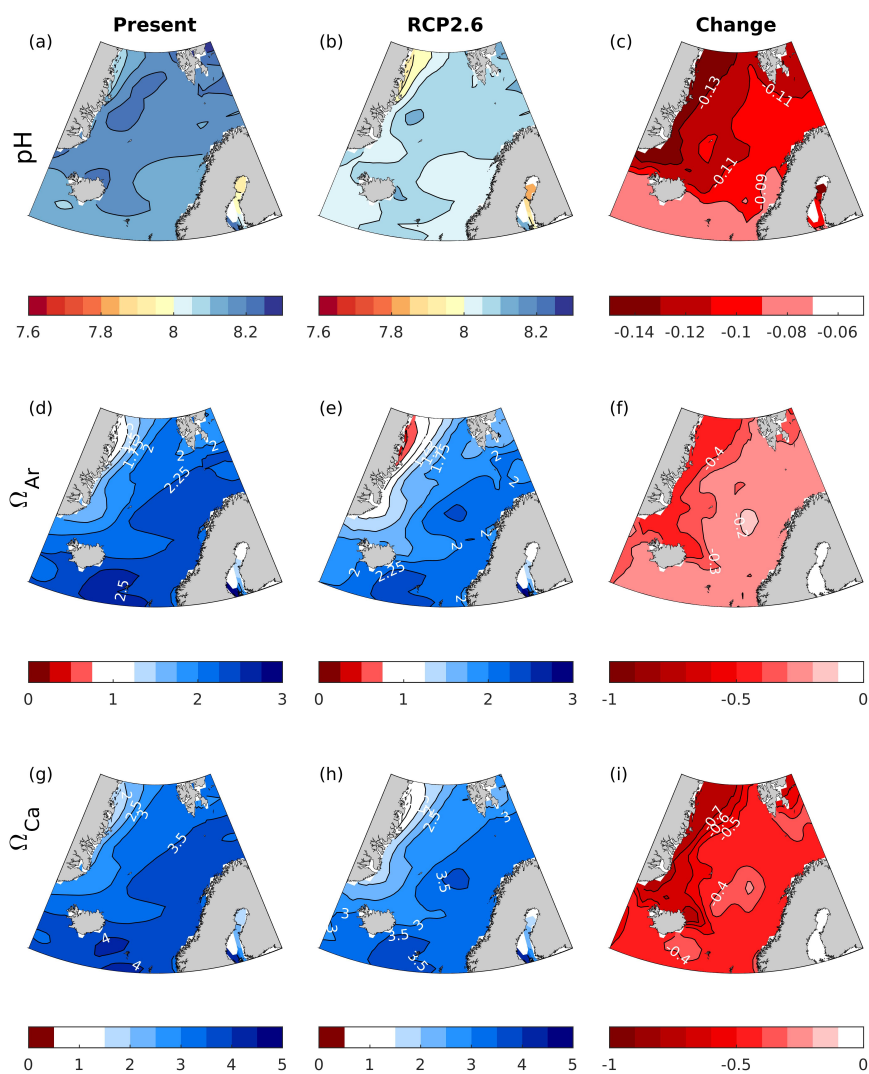
Figure 7. Maps of surface water pH, Ω_{Ar} and Ω_{Ca} for present (1980-2005) and future (2070-2099) for the RCP2.6 scenario, and the change in between, from the GLODAPv2 gridded climatologies combined with ocean acidification rates from the NorESM1-ME.

6 Discussion

6.1 Drivers of Ocean Acidification

Temperature, salinity, ALK and DIC are all affected by climate change, which can lead to changes in ocean pH that differ from
300   that expected by the CO_2 increase in the atmosphere alone. Further, when looking at decadal time scales as we have done in
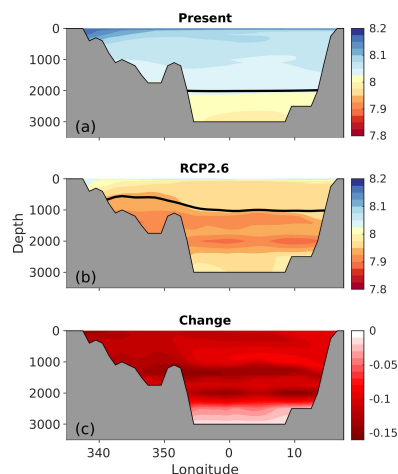
Figure 8. Zonal cross sections (at 70 °N) of present (1980-2005) and future (2070-2099) RCP2.6 pH, and the change between the periods. The solid black line shows the saturation horizon of aragonite (Ω_{Ar}=1).

Sect. 5.3, climate variability has a substantial impact on the temperature and salinity in the Nordic Seas (Furevik and Nilsen, 2013), and the potential to partly mask or amplify the effects of anthropogenic changes. In this section we therefore decompose the pH changes presented in Sect. 5 into its different drivers using Eq. 2 and subsequent transformation of fCO_2 to pH. We will focus on present changes, and put them into perspective of past and future changes.

305   The drivers of the observed changes in pH over the past decades (Sect. 5.3) are shown in Fig. 11, together with the expected change in pH assuming that the seawater pCO_2 perfectly tracks the change in atmospheric pCO_2 (black stars). Interbasin variations in the expected change are a result of variations in the buffer capacity. As seen in Fig. 11, the expected differences in pH decrease between the basins are relatively small. Any deviations of the observed changes from the black stars indicate that the change in seawater pCO_2 differs from that of the atmosphere.

310   In surface waters (the upper 200 m) the pH decrease is larger than expected from the increase in atmospheric CO_2 in all regions except for the Barents Sea Opening (denoted by the black stars in Fig. 11). This is related to a faster increase in the seawater pCO_2 compared with that of the atmosphere (Fig. S6), meaning that the pCO_2 undersaturation of the Nordic Seas is getting weaker. This has also been observed in earlier studies of the North Atlantic (Lefèvre et al., 2004; Olsen et al., 2006; Ólafsson et al., 2009; Metzl et al., 2010; Skjelvan et al., 2014). The mechanisms underlying the pCO_2 undersaturation in surface
315   waters of the Nordic Seas include strong primary production, cooling of northward flowing Atlantic waters, and the inflow of pCO_2 undersaturated waters from the Arctic Ocean (Olsen et al., 2008; Ólafsson et al., 2020b). A change in any of these factors could therefore result in a change in the pCO_2 difference between the atmosphere and the ocean. Considering that the samples we used are biased towards the productive season, it is possible that parts of the increase in the degree of pCO_2 saturation comes from the a reduction in the efficiency of the biological pump (i.e. biological CO_2 consumption), but it could also be a
320   result of warmer summer temperatures. The signal of increasing saturation gets stronger when only samples from June-August
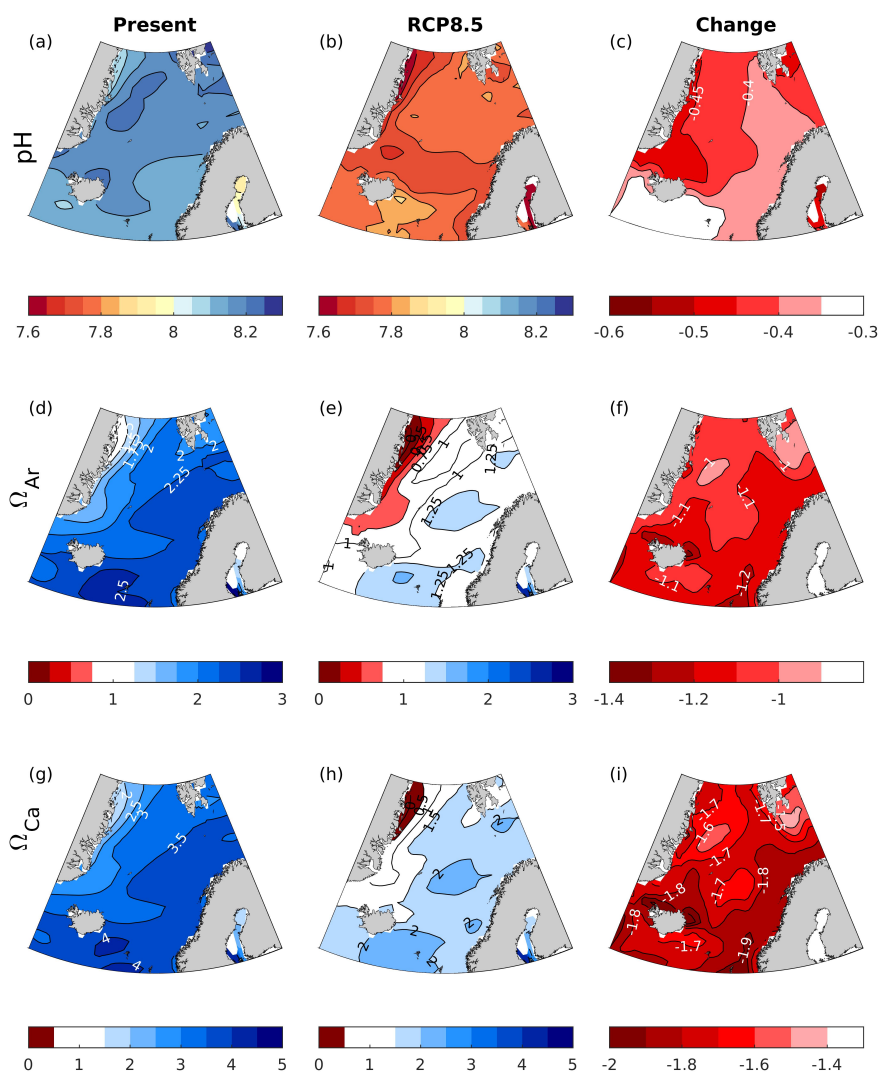
Figure 9. Maps of showing surface water pH, Ω_{Ar} and Ω_{Ca} for present (1980-2005) and for future (2070-2099) under the RCP8.5 scenario, and the change in between, from the GLODAPv2 gridded climatologies combined with ocean acidification rates from the NorESM1-ME.

are analyzed. Also Lefèvre et al. (2004) observed a stronger increase in the seawater pCO_2 during summer compared with winter in the North Atlantic subpolar gyre, which they suggested was a result of a decrease in productivity. The degree of undersaturation of surface waters could also be reduced as a result of a decreased cooling of northward flowing waters. This does not necessarily have to be seen in the local temperature, but can also be associated with changes in gradients of the atmospheric forcing along the flow path. One other possible mechanism was suggested in Olsen et al. (2006) and Anderson
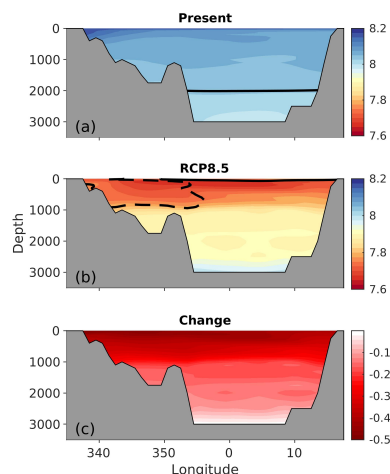
Figure 10. Zonal cross sections (at 70 °N) of present (1980-2005) and future RCP8.5 (2070-2099) pH, and the change between the periods. The solid and dashed black lines show the saturation horizons of aragonite and calcite, respectively (Ω_{Ar}=1 and Ω_{Ca}=1).

and Olsen (2002), where they associated the fast increase in seawater pCO_2 with a large advective supply of anthropogenic carbon from the south and corresponding changes in the buffer capacity. Further exploration of these various mechanisms is beyond the scope of this study.

The main driver of the pH decrease in the surface waters is an increase in DIC. This is partly offset by ALK increases
330 (see also Fig. S4). The effect of increasing ALK is strongest in the Barents Sea Opening and as such explains the low, non-significant, pH decline observed there (Fig. 5), while in the Norwegian Basin, the Lofoten Basin and Iceland Sea effects of changes in alkalinity are minor. The ALK increase is a consequence of the trend towards increasing salinities in the Nordic Seas in the past decades (Fig. S2). Increasing salinities in the Nordic Seas have been observed by many studies as a consequence of changes in the inflowing Atlantic Water related to subpolar gyre strength (Holliday et al., 2008; Lauvset et al., 2018). The
335 increasing salt content does not only affect ALK, but also equally DIC. Part of the reduction of pH from the DIC increase can therefore be attributed to the salinification. This effect is, however, about the same magnitude as the ALK driver, but in opposite direction (Fig. S8). The effects of changes in temperature on pH in surface waters are relatively small. In contrast to several studies pointing towards a warming of the Nordic Seas (e.g. Holliday et al., 2008; Blindheim and Østerhus, 2013; Lauvset et al., 2018; Ruiz-Barradas et al., 2018), all regions except for the Greenland Sea show a tendency towards a cooling
340 (Fig. S1), slightly increasing the pH, during this period of time. This can be a result of unequal distribution of sampling over the seasons, which should have the largest impact in surface waters.

The effect of increasing DIC is reduced away from the surface, a consequence of the gradual isolation of deeper waters from the atmosphere. DIC, however, remains the main driver of pH change down to 2000 meters depth, with a few exceptions. In the 200-500m layer in the Lofoten Basin and the Barents Sea Opening, there is an increase in temperature, leading to a pH
345 decline that is almost as large as that from the DIC increase. The overall warming seen in the deep waters is in accordance with
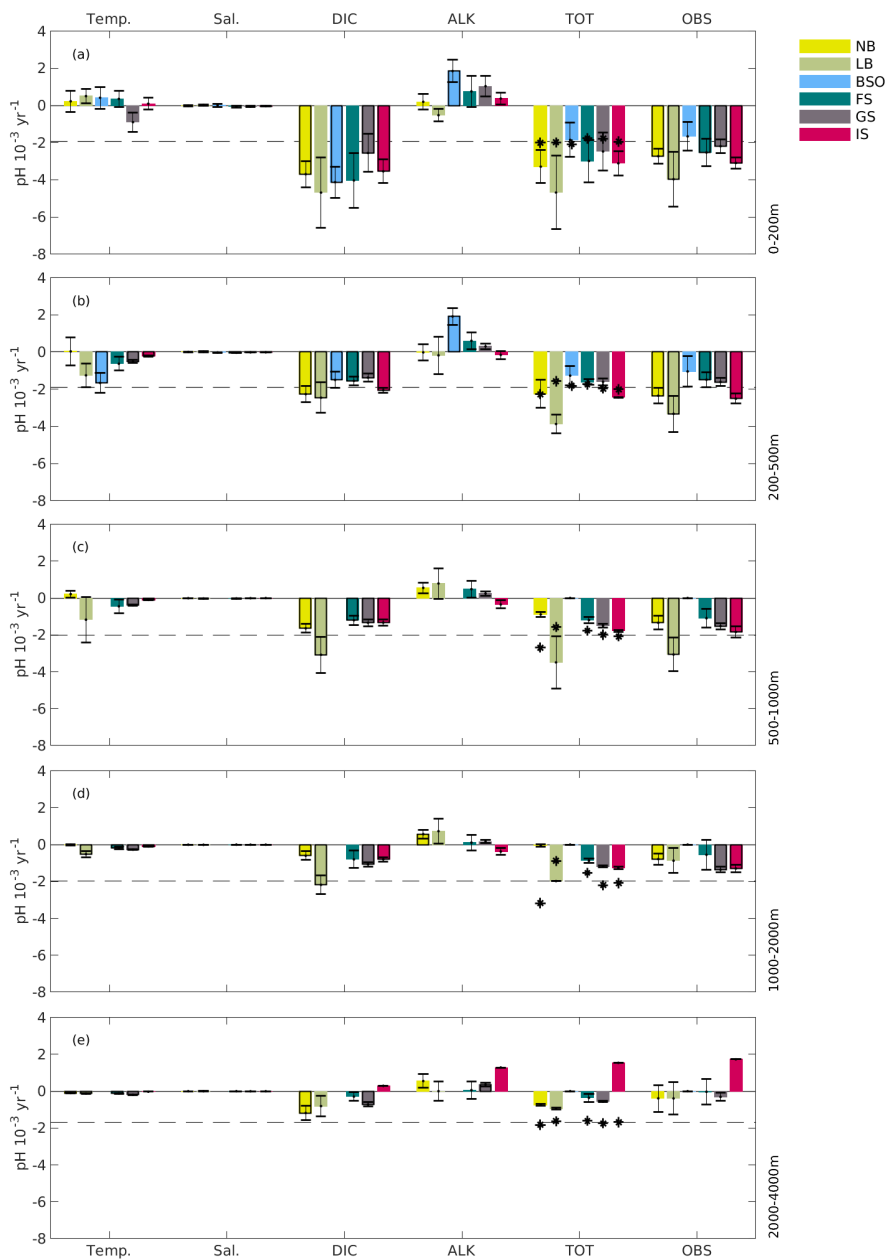
Figure 11. Contribution of observed changes in temperature, salinity, DIC, ALK to the observed trend in pH (OBS) over the 1981-2019 period. Bars showing trends that are significantly different from zero are outlined with a black line. TOT indicates the total trend in pH calculated as the sum of the trends associated with these four driving factors. The dashed line and black stars indicate the pH trend expected from the change in atmospheric CO_2 during the same period for the whole area and for the separate basins, respectively.

Østerhus and Gammelsrød (1999). The clear increase in ALK in the upper 500 m at the Barents Sea Opening dampens the effect of increasing DIC and temperature. In the 1000-2000m layer in the Norwegian Basin, there is an increase in ALK that cancels the effect of increasing DIC. Below 2000 meters, the effects of changes in ALK are of similar size as the effect of changes in DIC. It is interesting to note that the Lofoten Basin stands out as a region where the DIC and temperature signal reaches deeper than in other regions. This could be a result of a combination of the persistent eddy in the Lofoten Basin (dominating the upper 1000 m), and advection from the Greenland Sea intermediate water at about 1000-1500 m (Jeansson et al., 2017). However, a comparison like this should be taken with care because of the different lengths of the time series in the various regions.

Also for past and future changes in pH, the main driver is the change in DIC (Figs. S9-S11). In accordance with the observational dataset, no larger differences in pH change can be expected between the basins as a result of different buffer capacities. For the changes from pre-Industrial to present times, the effect of other factors than DIC are negligible. This explains the good agreement between the pre-Industrial modelled surface pH with the GLODAPv2 estimate (Fig. 2), where the latter one only takes into account DIC changes. In the RCP2.6 and 8.5 future scenarios (Figs. S10 and S11), the effects of increasing temperatures and ALK play a larger role, although they are still secondary to the effect of DIC. In the Iceland Sea, above 200 m, there is, in contrast to the other regions, a decrease in ALK in the RCP8.5 simulation, which has a negative impact on the pH. This is probably related to an increased export of freshwater from the Arctic Ocean (Shu et al., 2018).

Interestingly, as for the present days, the changes in pCO_2 under/oversaturation have substantial impact on the pH trends also during the past and the future scenarios. The pH decrease from past to present is not as large as expected from the change in atmospheric CO_2 due to an increase in the degree of CO_2 undersaturation. We relate this to a lag in the oceanic uptake of excess CO_2. The RCP2.6 scenario behaves differently. As there is a peak in atmospheric CO_2 in the middle of the 21st century and decrease thereafter, the seawater pCO_2 in the Nordic Seas catches up with that of the atmosphere, leading to a decrease in the degree of undersaturation in surface waters. In the RCP8.5 scenario the change in seawater pCO_2 also lags behind that of the atmosphere, with a few regional exceptions (note that this is difficult to see in Fig. S11 compared with Figs. S9 and S10 due to the different scale on the y-axis). The end-of-the-century DIC increase under the RCP2.6 scenario is larger in the deep than in the surface waters (Fig. S10), resulting in the stronger pH reduction at mid-depths as seen in Fig. 8. This is partly a result of the higher atmospheric CO_2 concentrations in the middle of the 21st century (Figs. 2 and S10); the waters at depth by the end-of-century were at the surface mid-century and exposed to peak atmospheric CO_2. This is demonstrated by the good agreement between observed pH change of deep waters, and the one expected from peak atmospheric CO_2 levels (Fig. S10). However, the large DIC increase in deep waters could also partly explained by increased remineralization. In both the RCP2.6 and RCP8.5 simulations there is an increase in the apparent oxygen utilization (AOU) from present to future all over the Nordic Seas at depths of 1800-2100 meters (not shown), indicating higher concentrations of carbon from the remineralization of organic matter. This could either be related to a larger production of organic matter or a slow down of the circulation. There is in particular a strong AOU increase in the deep Iceland Sea, explaining the large decrease in pH in these waters (Figs. S10 and S11).
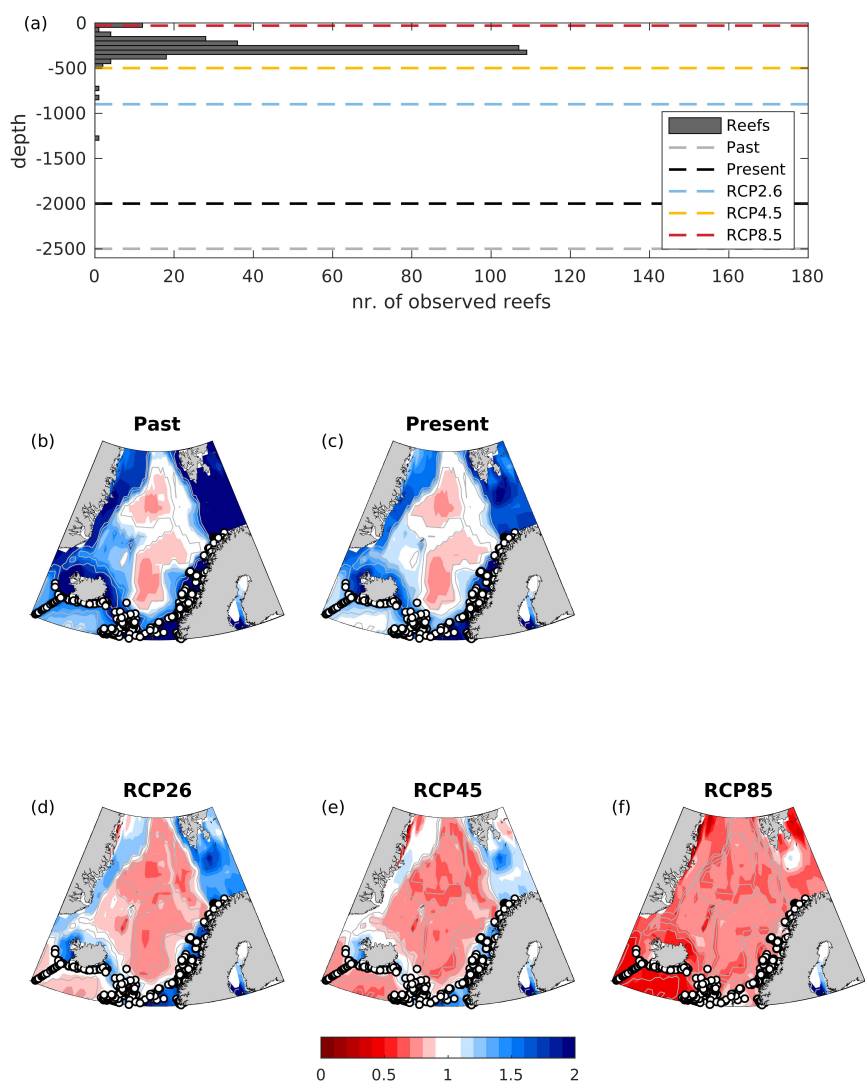
Figure 12. Number of observed reef sites per 100 m depth interval together with the saturation horizons (dashed lines) of aragonite in the Nordic Seas for past (1850-1879), present (1980-2005) and future (2070-2099) under the RCP2.6, RCP4.5 and RCP8.5 scenarios (a) and maps showing aragonite saturation state of bottom waters together with positions of observed reefs (b-f). The *Lophelia pertusa* reef locations were taken from OSPAR habitat maps.

6.2 Implications for cold-water corals

380   Cold-water corals build their structures with aragonite, which is the more soluble form of calcium carbonate. To some degree, the living coral can compensate for aragonite undersaturation in seawater by overriding their internal calcifying fluid, and

thus, increase their internal pH by 0.3-0.6 units (McCulloch et al., 2012; Allison et al., 2014). For some time these corals can therefore continue to calcify in waters with Ω_{Ar}<1. However, the calcification rates and breaking strength of the structures of the most abundant coral organism, *Lophelia pertusa*, is reduced if exposed to undersaturated waters (Hennige et al., 2015).

385 Furthermore, dead coral structures, which compose a major part of the reefs, cannot resist corrosive waters and experience increased dissolution rates in a situation with Ω_{Ar}<1, and, unavoidably the dead coral structures will slowly dissolve. The cold-water coral reefs, along with their ecosystems, are therefore likely to collapse if the water they live in becomes undersaturated in aragonite (Ω_{Ar}<1).

Most of the reefs that have been identified in the Nordic Seas (there are 324 in total withing the region defined in Fig. 1) are

390 at depths of 0-500 m, but there are also two that have been observed in depths ranges of 500-1000, and one reef in the range of 1000-2000 m (Fig. 12, see also Buhl-Mortensen et al. (2015)). At present, the saturation horizon with respect to aragonite is found deeper than the cold-water corals in the Nordic Seas, but the waters in the depth range of 1000-2000 m are close to being undersaturated in aragonite (Sect. 5.3). However, the one reef in the Nordic Seas that is found below 1000 m of depth is located near the Faroe Islands, and is relatively far from the regions that we have analyzed for the present day acidification. It

395 is therefore difficult to draw any conclusions on whether this reef is close to being exposed to corrosive waters or not. In the RCP2.6 and RCP4.5 scenarios, NorESM1-ME projects that the aragonite saturation horizon will be lifted to 900 m and 500 m, respectively, by the end of the 21st century. This implies that the deepest observed reefs will be exposed to Ω_{Ar}<1, and thus, experience elevated costs of calcification. In the RCP8.5 scenario all cold-water coral reefs below 30 m (97%) depth in the Nordic Seas are projected to be exposed to aragonite undersaturation.

400 7 Conclusions

In this study we have provided a detailed investigation of spatial and temporal variations of the past, ongoing and future acidification, and its drivers, in the Nordic Seas. We have further assessed the potential impacts of this acidification on aragonite saturation and cold-water coral reefs. From 1850-1980 both model simulation and observational data together with the GLODAPv2 pre-Industrial estimate, suggest that the pH of the Nordic Seas surface waters has dropped by 0.05 units, which is

405 similar to the pH decrease of the global surface ocean. During this time period the aragonite saturation horizon has slightly shallowed, but has remained well below the depths of known cold-water coral habitats. During the last 40 years, when regular sampling of carbon system parameters have been made in the region, the pH of the Nordic Seas surface waters has decreased with a rate of -2.79±0.3 mpH yr^{-1} on average, resulting in a drop of 0.11 units. This trend is stronger than the trend observed for the global ocean of -0.18±0.4 mpH yr^{-1} for the period 1991-2011 (Lauvset et al., 2015). The pH reductions are signif-

410 icant all over the Nordic Seas, except for the Barents Sea Opening, where it has been minimized by an exceptionally strong increase in ALK. In some regions the acidification signal is detectable down to 2000 m. During these last 40 years the waters at 1000-2000 m have approached undersaturation in aragonite. Future scenarios suggest an additional pH drop of 0.1-0.4 units in the surface waters. In the worst case scenario, RCP8.5, all cold-water coral reefs will be exposed to corrosive waters by the end of the 21st century, threatening not only their existence, but also that of their associated ecosystems. The NorESM1-ME
415 simulations suggest that this can largely be avoided by keeping the emissions within the limits set by the RCP4.5 scenario. It is, however, important to keep in mind that the future location of the saturation horizon is undoubtedly dependent on the model's ability to represent deep water masses and their separate formation processes, which is subject to large inter-model variations. More studies are therefore needed to verify the sensitivity of these results to model bias.

The drop in pH is mainly driven by an increase in DIC for all time periods. In the last 40 years, it has been slightly reinforced

420 by a warming (except in surface waters) and opposed by an increase in ALK. The RCP2.6 and RCP8.5 scenarios suggest that the effect of increasing temperatures and alkalinities will be stronger in the future, but such effects still only play a secondary role to DIC increase. The direct effect of changes in salinity on pH only play a minor role for the pH change in the Nordic Seas.

For both past, present and future, we find that the pCO_2 difference between the seawater and the atmosphere is not constant

425 and varies both in space and time. This gives rise to spatial variations in acidification rates within the Nordic Seas that are larger than expected from the local water mass composition and buffer capacity. It also explains the difference in the pH drops between the global ocean and the Nordic Seas. This includes the rapid acidification rate of the Nordic Seas surface waters during the past 40 years, when there has been a decrease in the degree of pCO_2 undersaturation of the surface waters. Clearly, more research on the processes governing the Nordic Seas surface water pCO_2 is needed, not only to understand the pH

430 dynamics of the Nordic Seas, but also its role as a CO_2 sink.

Data availability. The GLODAPv2.2019 data and GLODAPv2 mapped climatologies are available for download at
https://www.glodap.info/index.php/merged-and-adjusted-data-product-v2-2019/
and https://www.glodap.info/index.php/mapped-data-product/ , respectively.

The data from Ocean Weather station M from 2001-2007 is available in GLODAPv2.2019. Data from the time period 2008-2019 will be

435 available in the next GLODAP version.

The data from the time series station in the Iceland Sea can be obtained from the NCEI database (Ólafsson, 2012; Ólafsdóttir et al., 2020)

The data from the Norwegian ocean acidification monitoring program (Chierici et al., 2019a), and from the Eastern Fram Strait (Chierici and Fransson, 2019) is available at the Norwegian Marine Data Centre (NMDC).

The NorESM1-ME simulations can be downloaded at https://esgf-node.llnl.gov/search/cmip5/

440 *Author contributions.* AO, FF and FF designed the research. FF, FF, and AO performed the data-analysis with inputs from IS, MC and EJ. FF lead the writing of the manuscript with inputs from all co-authors. JT designed, tested, and performed the NorESM1-ME model simulations.

Competing interests. The authors declare that they have no conflict of interest.

Acknowledgements. Filippa Fransner and Friederike Fröb were funded by the Bjerknes Centre for Climate Research. JT acknowledges

445   funding from Research Council of Norway (Reef-Futures no. 295349 and Columbia no. 275268). SKL acknowledges funding from the
Research Council of Norway (NorArgo2, 269753) High-performance computing and storage resources were provided by the Norwegian
infrastructure for computational science (through projects nn1002k and ns1002k). The Norwegian Ocean Acidification Monitoring Program
is funded by the Norwegian Environmental Agency through project no. 17078007. The flagship program" Ocean acidification and effects in
northern waters" within the FRAM-High North Research Centre for Climate and the Environment.

450 **References**

Allison, N., Cohen, I., Finch, A., Erez, J., and Tudhope, A.: Corals concentrate dissolved inorganic carbon to facilitate calcification, Nature
    Communications, 5, https://doi.org/doi:10.1038/ncomms6741, 2014.

Anderson, L. G. and Olsen, A.: Air–sea flux of anthropogenic carbon dioxide in the North Atlantic, Geophysical Research Letters, 29,
    16–1–16–4, https://doi.org/10.1029/2002GL014820, https://agupubs.onlinelibrary.wiley.com/doi/abs/10.1029/2002GL014820, 2002.

455 Bentsen, M., Bethke, I., Debernard, J. B., Iversen, T., Kirkevåg, A., Seland, Ø., Drange, H., Roelandt, C., Seierstad, I. A., Hoose, C., and
    Kristjánsson, J. E.: The Norwegian Earth System Model, NorESM1-M – Part 1: Description and basic evaluation of the physical climate,
    Geoscientific Model Development, 6, 687–720, https://doi.org/10.5194/gmd-6-687-2013, https://gmd.copernicus.org/articles/6/687/2013/,
    2013.

Bleck, R. and Smith, L. T.: A wind-driven isopycnic coordinate model of the north and equatorial Atlantic Ocean: 1. Model development
460   and supporting experiments, Journal of Geophysical Research: Oceans, 95, 3273–3285, https://doi.org/10.1029/JC095iC03p03273, https:
    //agupubs.onlinelibrary.wiley.com/doi/abs/10.1029/JC095iC03p03273, 1990.

Blindheim, J.: Arctic intermediate water in the Norwegian sea, Deep Sea Research Part A. Oceanographic Research Pa-
    pers, 37, 1475 – 1489, https://doi.org/https://doi.org/10.1016/0198-0149(90)90138-L, http://www.sciencedirect.com/science/article/pii/
    019801499090138L, 1990.

465 Blindheim, J. and Østerhus, S.: The Nordic Seas, Main Oceanographic Features, pp. 11–37, American Geophysical Union (AGU),
    https://doi.org/10.1029/158GM03, https://agupubs.onlinelibrary.wiley.com/doi/abs/10.1029/158GM03, 2013.

Blindheim, J. and Rey, F.: Water-mass formation and distribution in the Nordic Seas during the 1990s, ICES Journal of Marine Science, 61,
    846–863, https://doi.org/10.1016/j.icesjms.2004.05.003, https://doi.org/10.1016/j.icesjms.2004.05.003, 2004.

Bopp, L., Resplandy, L., Orr, J. C., Doney, S. C., Dunne, J. P., Gehlen, M., Halloran, P., Heinze, C., Ilyina, T., Séférian, R., Tjiputra, J., and
470   Vichi, M.: Multiple stressors of ocean ecosystems in the 21st century: projections with CMIP5 models, Biogeosciences, 10, 6225–6245,
    https://doi.org/10.5194/bg-10-6225-2013, https://bg.copernicus.org/articles/10/6225/2013/, 2013.

Brakstad, A., Våge, K., Håvik, L., and Moore, G. W. K.: Water Mass Transformation in the Greenland Sea during the Period 1986–2016, Jour-
    nal of Physical Oceanography, 49, 121–140, https://doi.org/10.1175/JPO-D-17-0273.1, https://doi.org/10.1175/JPO-D-17-0273.1, 2019.

Buhl-Mortensen, L., Olafsdottir, S. H., Buhl-Mortensen, P., Burgos, J. M., and Ragnarsson, S. A.: Distribution of nine cold-water coral
475   species (Scleractinia and Gorgonacea) in the cold temperate North Atlantic: effects of bathymetry and hydrography, Hydrobiologia, 759,
    39–61, https://doi.org/10.1007/s10750-014-2116-x, https://doi.org/10.1007/s10750-014-2116-x, 2015.

Caldeira, K. and Wickett, M. E.: Anthropogenic carbon and ocean pH, Nature, 425, 365–365, https://doi.org/10.1038/425365a, https://doi.
    org/10.1038/425365a, 2003.

Chafik, L. and Rossby, T.: Volume, Heat, and Freshwater Divergences in the Subpolar North Atlantic Suggest the Nordic Seas as Key to the
480   State of the Meridional Overturning Circulation, Geophysical Research Letters, 46, 4799–4808, https://doi.org/10.1029/2019GL082110,
    https://agupubs.onlinelibrary.wiley.com/doi/abs/10.1029/2019GL082110, 2019.

Chierici, M. and Fransson, A.: Seasonal variability of the marine CO_2 system and nutrients in the Atlantic water inflow to the Arctic Ocean
    in 2014, https://doi.org/10.21335/NMDC-154415697, dataset, 2019.

Chierici, M., Sørensen, K., Johannessen, T., Børsheim, K., A.Olsen, Yakushev, E., Omar, A., and Blakseth, T.: Tillførselprogrammet 2011,
485   Overvåking av havsforsuring av norske farvann. Rapport, Klif, TA2936-2012, Tech. rep., 2012.

Chierici, M., Sørensen, K., Johannessen, T., Børsheim, K., A.Olsen, Yakushev, E., Omar, A., Skjelvan, I., Norli, M., , and Lauvset, S.: Tillførselprogrammet 2012, Overvåking av havsforsuring av norske farvann. Rapport, Klif, TA3043-2013, Tech. rep., 2013.

Chierici, M., Skjelvan, I., Bellerby, R., M. Norli, L. F., Hodal, H., Børsheim, K., Lauvset, S., Johannessen, T., Sørensen, K., and Yakushev, E.: Overvåking av havforsuring av norske farvann. Rapport, Miljødirektoratet M-218, Tech. rep., 2014.

490   Chierici, M., Skjelvan, I., Norli, M., Lødemel, H., Lunde, L., Sørensen, K., Yakushev, E., Bellerby, R., King, A., Lauvset, S., Johannessen, T., and Børsheim, K.: Overvåking av havforsuring i norske farvann i 2014, Rapport, Miljødirektoratet, M-354, Tech. rep., 2015.

Chierici, M., Skjelvan, I., Norli, M., Børsheim, K., Lauvset, S., Lødemel, H., Sørensen, K., King, A., Kutti, T., Renner, A., Omar, A., and Johannessen, T.: Overvåking av havforsuring i norske farvann i 2015, Rapport, Miljødirektoratet, M-573, Tech. rep., 2016.

Chierici, M., Skjelvan, I., Norli, M., Jones, E., Børsheim, K., Lauvset, S., Lødemel, H., Sørensen, K., King, A., and Johannessen, T.:
495   Overvåking av havforsuring i norske farvann i 2016, Rapport, Miljødirektoratet, M-776, Tech. rep., 2017.

Chierici, M., Jones, E., and Lødemel, H. H.: Interannual variability of the marine CO_2 system and nutrients in the Norwegian Sea from 2011 to 2017, https://doi.org/10.21335/NMDC-1939716216, dataset, 2019a.

Chierici, M., Vernet, M., Fransson, A., and Børsheim, K. Y.: Net Community Production and Carbon Exchange From Winter to Summer in the Atlantic Water Inflow to the Arctic Ocean, Frontiers in Marine Science, 6, 528, https://doi.org/10.3389/fmars.2019.00528, https:
500   //www.frontiersin.org/article/10.3389/fmars.2019.00528, 2019b.

Dai, A., Luo, D., Song, M., and Liu, J.: Arctic amplification is caused by sea-ice loss under increasing CO2, Nature Communications, 10, 121, https://doi.org/10.1038/s41467-018-07954-9, https://doi.org/10.1038/s41467-018-07954-9, 2019.

Dickson, A. G.: Standard potential of the reaction: AgCl(s) + 12H2(g) = Ag(s) + HCl(aq), and and the standard acid-ity constant of the ion HSO4- in synthetic sea water from 273.15 to 318.15 K, The Journal of Chemical Thermodynam-
505   ics, 22, 113 – 127, https://doi.org/https://doi.org/10.1016/0021-9614(90)90074-Z, http://www.sciencedirect.com/science/article/pii/0021961490090074Z, 1990.

Dickson, R. R. and Brown, J.: The production of North Atlantic Deep Water: Sources, rates, and pathways, Journal of Geophysical Research: Oceans, 99, 12 319–12 341, https://doi.org/10.1029/94JC00530, https://agupubs.onlinelibrary.wiley.com/doi/abs/10.1029/94JC00530, 1994.

510   Doney, S. C., Fabry, V. J., Feely, R. A., and Kleypas, J. A.: Ocean Acidification: The Other CO_2 Problem, Annual Review of Marine Science, 1, 169–192, https://doi.org/10.1146/annurev.marine.010908.163834, https://doi.org/10.1146/annurev.marine.010908.163834, pMID: 21141034, 2009.

Doney, S. C., Busch, D. S., Cooley, S. R., and Kroeker, K. J.: The Impacts of Ocean Acidification on Marine Ecosystems and Reliant Human Communities, Annual Review of Environment and Resources, 45, null, https://doi.org/10.1146/annurev-environ-012320-083019,
515   https://doi.org/10.1146/annurev-environ-012320-083019, 2020.

Doo, S. S., Kealoha, A., Andersson, A., Cohen, A. L., Hicks, T. L., Johnson, Z. I., Long, M. H., McElhany, P., Mollica, N., Shamberger, K. E. F., Silbiger, N. J., Takeshita, Y., and Busch, D. S.: The challenges of detecting and attributing ocean acidification impacts on marine ecosystems, ICES Journal of Marine Science, https://doi.org/10.1093/icesjms/fsaa094, https://doi.org/10.1093/icesjms/fsaa094, fsaa094, 2020.

520   Friedlingstein, P., Jones, M. W., O'Sullivan, M., Andrew, R. M., Hauck, J., Peters, G. P., Peters, W., Pongratz, J., Sitch, S., Le Quéré, C., Bakker, D. C. E., Canadell, J. G., Ciais, P., Jackson, R. B., Anthoni, P., Barbero, L., Bastos, A., Bastrikov, V., Becker, M., Bopp, L., Buitenhuis, E., Chandra, N., Chevallier, F., Chini, L. P., Currie, K. I., Feely, R. A., Gehlen, M., Gilfillan, D., Gkritzalis, T., Goll, D. S., Gruber, N., Gutekunst, S., Harris, I., Haverd, V., Houghton, R. A., Hurtt, G., Ilyina, T., Jain, A. K., Joetzjer, E., Kaplan, J. O., Kato, E.,

Klein Goldewijk, K., Korsbakken, J. I., Landschützer, P., Lauvset, S. K., Lefèvre, N., Lenton, A., Lienert, S., Lombardozzi, D., Marland,
525 G., McGuire, P. C., Melton, J. R., Metzl, N., Munro, D. R., Nabel, J. E. M. S., Nakaoka, S.-I., Neill, C., Omar, A. M., Ono, T., Peregon,
A., Pierrot, D., Poulter, B., Rehder, G., Resplandy, L., Robertson, E., Rödenbeck, C., Séférian, R., Schwinger, J., Smith, N., Tans, P. P.,
Tian, H., Tilbrook, B., Tubiello, F. N., van der Werf, G. R., Wiltshire, A. J., and Zaehle, S.: Global Carbon Budget 2019, Earth System
Science Data, 11, 1783–1838, https://doi.org/10.5194/essd-11-1783-2019, https://essd.copernicus.org/articles/11/1783/2019/, 2019.

Furevik, T. and Nilsen, J. E. Ø.: Large-Scale Atmospheric Circulation Variability and its Impacts on the Nordic Seas Ocean Climate—A
530 Review, pp. 105–136, American Geophysical Union (AGU), https://doi.org/10.1029/158GM09, https://agupubs.onlinelibrary.wiley.com/
doi/abs/10.1029/158GM09, 2013.

Gattuso, J.-P. and Hansson, L.: Ocean acidification: background and history, In Ocean Acidification, ed. J-P Gattuso, L Hansson, pp. 1–20,
Oxford University Press, Oxford, UK, 2011.

Gehlen, M., Séférian, R., Jones, D. O. B., Roy, T., Roth, R., Barry, J., Bopp, L., Doney, S. C., Dunne, J. P., Heinze, C., Joos, F., Orr, J. C.,
535 Resplandy, L., Segschneider, J., and Tjiputra, J.: Projected pH reductions by 2100 might put deep North Atlantic biodiversity at risk,
Biogeosciences, 11, 6955–6967, https://doi.org/10.5194/bg-11-6955-2014, https://bg.copernicus.org/articles/11/6955/2014/, 2014.

Guinotte, J. M., Orr, J., Cairns, S., Freiwald, A., Morgan, L., and George, R.: Will human-induced changes in seawater chemistry alter
the distribution of deep-sea scleractinian corals?, Frontiers in Ecology and the Environment, 4, 141–146, https://doi.org/10.1890/1540-
9295(2006)004[0141:WHCISC]2.0.CO;2, 2006.

540 Hansen, B. and Østerhus, S.: North Atlantic–Nordic Seas exchanges, Progress in Oceanography, 45, 109 – 208,
https://doi.org/https://doi.org/10.1016/S0079-6611(99)00052-X, http://www.sciencedirect.com/science/article/pii/S007966119900052X,
2000.

Hennige, S. J., Wicks, L. C., Kamenos, N. A., Perna, G., Findlay, H. S., and Roberts, J. M.: Hidden impacts of ocean acidification to live and
dead coral framework, Proceedings of the Royal Society B: Biological Sciences, 282, 20150 990, https://doi.org/10.1098/rspb.2015.0990,
545 https://royalsocietypublishing.org/doi/abs/10.1098/rspb.2015.0990, 2015.

Holliday, N. P., Hughes, S. L., Bacon, S., Beszczynska-Möller, A., Hansen, B., Lavín, A., Loeng, H., Mork, K. A., Østerhus, S., Sherwin,
T., and Walczowski, W.: Reversal of the 1960s to 1990s freshening trend in the northeast North Atlantic and Nordic Seas, Geophysical
Research Letters, 35, https://doi.org/10.1029/2007GL032675, https://agupubs.onlinelibrary.wiley.com/doi/abs/10.1029/2007GL032675,
2008.

550 IPCC: Climate Change 2014: Synthesis Report. Contribution of Working Groups I, II and III to the Fifth Assessment Report of the Intergov-
ernmental Panel on Climate Change, [Core Writing Team, R.K. Pachauri and L.A. Meyer (eds.)], Tech. rep., IPCC, Geneva, Switzerland,
2014.

Jeansson, E., Olsen, A., Eldevik, T., Skjelvan, I., Omar, A. M., Lauvset, S. K., Nilsen, J. E. Ø., Bellerby, R. G. J., Johan-
nessen, T., and Falck, E.: The Nordic Seas carbon budget: Sources, sinks, and uncertainties, Global Biogeochemical Cycles, 25,
555 https://doi.org/10.1029/2010GB003961, https://agupubs.onlinelibrary.wiley.com/doi/abs/10.1029/2010GB003961, 2011.

Jeansson, E., Olsen, A., and Jutterström, S.: Arctic Intermediate Water in the Nordic Seas, 1991–2009, Deep Sea Research Part I: Oceano-
graphic Research Papers, 128, 82 – 97, https://doi.org/https://doi.org/10.1016/j.dsr.2017.08.013, http://www.sciencedirect.com/science/
article/pii/S0967063716300668, 2017.

Jiang, L.-Q., Carter, B. R., Feely, R. A., Lauvset, S. K., and Olsen, A.: Surface ocean pH and buffer capacity: past, present and future,
560 Scientific Reports, 9, 18 624, https://doi.org/10.1038/s41598-019-55039-4, https://doi.org/10.1038/s41598-019-55039-4, 2019.

Jones, E., Chierici, M., Skjelvan, I., M. Norli, K. B., Lødemel, H., Kutti, T., Sørensen, K., King, A., Jackson, K., and de Lange, T.: Monitoring of the ocean acidification in Norwegian seas in 2017, Report, Miljødirektoratet, M-1072, Tech. rep., 2018.

Jones, E., Chierici, M., Skjelvan, I., Norli, M., Børsheim, K., Lødemel, H., Sørensen, K., King, A., Lauvset, S., Jackson, K., de Lange, T., Johannssessen, T., and Mourgues, C.: Monitoring ocean acidification in Norwegian seas in 2018, Rapport, Miljødirektoratet, M-1417, Tech. rep., 2019.

Jones, E., Chierici, M., Skjelvan, I., Norli, M., Frigstad, H., Børsheim, K., Lødemel, H., Kutti, T., King, A., Sørensen, K., Lauvset, S., Jackson-Misje, K., Apelthun, L., de Lange, T., Johannssessen, T., Mourgues, C., and Bellerby, R.: Monitoring ocean acidification in Norwegian seas in 2019, Rapport, Miljødirektoratet, M-1735, Tech. rep., 2020.

Jutterström, S. and Jeansson, E.: Anthropogenic carbon in the East Greenland Current, Progress in Oceanography, 78, 29 – 36, https://doi.org/https://doi.org/10.1016/j.pocean.2008.04.001, http://www.sciencedirect.com/science/article/pii/S0079661108000876, 2008.

Kutti, T., Bergstad, O. A., Fosså, J. H., and Helle, K.: Cold-water coral mounds and sponge-beds as habitats for demersal fish on the Norwegian shelf, Deep Sea Research Part II: Topical Studies in Oceanography, 99, 122 – 133, https://doi.org/https://doi.org/10.1016/j.dsr2.2013.07.021, http://www.sciencedirect.com/science/article/pii/S0967064513002956, biology and Geology of Deep-Sea Coral Ecosystems: Proceedings of the Fifth International Symposium on Deep Sea Corals, 2014.

Kwiatkowski, L., Torres, O., Bopp, L., Aumont, O., Chamberlain, M., Christian, J. R., Dunne, J. P., Gehlen, M., Ilyina, T., John, J. G., Lenton, A., Li, H., Lovenduski, N. S., Orr, J. C., Palmieri, J., Santana-Falcón, Y., Schwinger, J., Séférian, R., Stock, C. A., Tagliabue, A., Takano, Y., Tjiputra, J., Toyama, K., Tsujino, H., Watanabe, M., Yamamoto, A., Yool, A., and Ziehn, T.: Twenty-first century ocean warming, acidification, deoxygenation, and upper-ocean nutrient and primary production decline from CMIP6 model projections, Biogeosciences, 17, 3439–3470, https://doi.org/10.5194/bg-17-3439-2020, https://bg.copernicus.org/articles/17/3439/2020/, 2020.

Lauvset, S. K., Gruber, N., Landschützer, P., Olsen, A., and Tjiputra, J.: Trends and drivers in global surface ocean pH over the past 3 decades, Biogeosciences, 12, 1285–1298, https://doi.org/10.5194/bg-12-1285-2015, https://bg.copernicus.org/articles/12/1285/2015/, 2015.

Lauvset, S. K., Key, R. M., Olsen, A., van Heuven, S., Velo, A., Lin, X., Schirnick, C., Kozyr, A., Tanhua, T., Hoppema, M., Jutterström, S., Steinfeldt, R., Jeansson, E., Ishii, M., Perez, F. F., Suzuki, T., and Watelet, S.: A new global interior ocean mapped climatology: the 1° × 1° GLODAP version 2, Earth System Science Data, 8, 325–340, https://doi.org/10.5194/essd-8-325-2016, https://essd.copernicus.org/articles/8/325/2016/, 2016.

Lauvset, S. K., Brakstad, A., Våge, K., Olsen, A., Jeansson, E., and Mork, K. A.: Continued warming, salinification and oxygenation of the Greenland Sea gyre, Tellus A: Dynamic Meteorology and Oceanography, 70, 1–9, https://doi.org/10.1080/16000870.2018.1476434, https://doi.org/10.1080/16000870.2018.1476434, 2018.

Lefèvre, N., Watson, A. J., Olsen, A., Ríos, A. F., Pérez, F. F., and Johannessen, T.: A decrease in the sink for atmospheric CO_2 in the North Atlantic, Geophysical Research Letters, 31, https://doi.org/10.1029/2003GL018957, https://agupubs.onlinelibrary.wiley.com/doi/abs/10.1029/2003GL018957, 2004.

Lewis, E. and Wallace, D. W. R.: Program Developed for CO_2 System Calculations, ORNL/CDIAC-105. Carbon Dioxide Information Analysis Center, Oak Ridge National Laboratory, US Department of Energy, Oak Ridge, Tennessee., 1998.

Lueker, T. J., Dickson, A. G., and Keeling, C. D.: Ocean pCO_2 calculated from dissolved inorganic carbon, alkalinity, and equations for K1 and K2: validation based on laboratory measurements of CO_2 in gas and seawater at equilibrium, Marine Chemistry, 70, 105 – 119, https://doi.org/https://doi.org/10.1016/S0304-4203(00)00022-0, http://www.sciencedirect.com/science/article/pii/S0304420300000220, 2000.

Maier-Reimer, E., Kriest, I., Segschneider, J., and Wetzel, P.: The HAMburg Ocean Carbon Cycle Model HAMOCC5.1 - Technical Descrip-
600   tion Release 1.1.Berichte zur Erdsystemforschung, 14., Tech. rep., 2005.

McCulloch, M., Trotter, J., Montagna, P., Falter, J., Dunbar, R., Freiwald, A., Försterra, G., López Correa, M., Maier, C., Rüggeberg,
A., and Taviani, M.: Resilience of cold-water scleractinian corals to ocean acidification: Boron isotopic systematics of pH and saturation
state up-regulation, Geochimica et Cosmochimica Acta, 87, 21 – 34, https://doi.org/https://doi.org/10.1016/j.gca.2012.03.027, http://www.
sciencedirect.com/science/article/pii/S001670371200169X, 2012.

605   Messias, M.-J., Watson, A., Johannessen, T., Oliver, K., Olsson, K., Fogelqvist, E., Olafsson, J., Bacon, S., Balle, J., Bergman, N., Budéus, G.,
Danielsen, M., Gascard, J.-C., Jeansson, E., Olafsdottir, S., Simonsen, K., Tanhua, T., Van Scoy, K., and Ledwell, J.: The Greenland Sea
tracer experiment 1996–2002: Horizontal mixing and transport of Greenland Sea Intermediate Water, Progress in Oceanography, 78, 85 –
105, https://doi.org/https://doi.org/10.1016/j.pocean.2007.06.005, http://www.sciencedirect.com/science/article/pii/S0079661108000852,
2008.

610   Metzl, N., Corbière, A., Reverdin, G., Lenton, A., Takahashi, T., Olsen, A., Johannessen, T., Pierrot, D., Wanninkhof, R., Ólafsdót-
tir, S. R., Olafsson, J., and Ramonet, M.: Recent acceleration of the sea surface fCO_2 growth rate in the North Atlantic subpo-
lar gyre (1993–2008) revealed by winter observations, Global Biogeochemical Cycles, 24, https://doi.org/10.1029/2009GB003658,
https://agupubs.onlinelibrary.wiley.com/doi/abs/10.1029/2009GB003658, 2010.

Ólafsdóttir, S. R., Benoit-Cattin, A., and Danielsen, M.: Dissolved inorganic carbon (DIC), total alkalinity, temperature, salinity, nutrients
615   and dissolved oxygen collected from discrete samples and profile observations during the R/Vs Arni Fridriksson and Bjarni Saemundsson
time series IcelandSea (LN6) cruises in the North Atlantic Ocean from 2014-02-18 to 2019-10-31 (NCEI Accession 0209074), https:
//doi.org/10.25921/qhed-3h84, dataset, 2020.

Ólafsson, J.: Winter mixed layer nutrients in the Irminger and Iceland Seas,1990-2000, ICES Marine Science Symposia, 219, 2003.

Ólafsson, J.: Partial pressure (or fugacity) of carbon dioxide, dissolved inorganic carbon, temperature, salinity and other variables collected
620   from discrete samples, profile and time series profile observations during the R/Vs Arni Fridriksson and Bjarni Saemundsson time series
IcelandSea (LN6) cruises in the North Atlantic Ocean from 1985-02-22 to 2013-11-26 (NCEI Accession 0100063), https://doi.org/10.
3334/cdiac/otg.carina_icelandsea, dataset, 2012.

Ólafsson, J., Ólafsdóttir, S., Benoit-Cattin, A., Danielsen, M., Arnarson, T. S., and Takahashi, T.: Rate of Iceland Sea acidification from time
series measurements, Biogeosciences, 6, 2661–2668, 2009.

625   Ólafsson, J., Lee, K., Ólafsdóttir, S. R., Benoit-Cattin, A., Lee, C.-H., and Kim, M.: Boron to salinity ratios for Atlantic, Arctic and Polar
Waters: A view from downstream, Marine Chemistry, 224, 103 809, https://doi.org/https://doi.org/10.1016/j.marchem.2020.103809, http:
//www.sciencedirect.com/science/article/pii/S0304420320300633, 2020a.

Ólafsson, J., Ólafsdóttir, S. R., Takahashi, T., Danielsen, M., and Arnarson, T. S.: Enhancement of the North Atlantic CO_2 sink by Arctic
Waters, Biogeosciences Discussions, 2020, 1–21, https://doi.org/10.5194/bg-2020-313, https://bg.copernicus.org/preprints/bg-2020-313/,
630   2020b.

Olsen, A., Omar, A. M., Bellerby, R. G. J., Johannessen, T., Ninnemann, U., Brown, K. R., Olsson, K. A., Olafsson, J., Nondal, G., Kivimäe,
C., Kringstad, S., Neill, C., and Olafsdottir, S.: Magnitude and origin of the anthropogenic CO_2 increase and 13C Suess effect in the
Nordic seas since 1981, Global Biogeochemical Cycles, 20, https://doi.org/10.1029/2005GB002669, https://agupubs.onlinelibrary.wiley.
com/doi/abs/10.1029/2005GB002669, 2006.

635   Olsen, A., Brown, K. R., Chierici, M., Johannessen, T., and Neill, C.: Sea-surface CO_2 fugacity in the subpolar North Atlantic, Biogeo-
sciences, 5, 535–547, https://doi.org/10.5194/bg-5-535-2008, https://bg.copernicus.org/articles/5/535/2008/, 2008.

Olsen, A., Lange, N., Key, R. M., Tanhua, T., Álvarez, M., Becker, S., Bittig, H. C., Carter, B. R., Cotrim da Cunha, L., Feely, R. A., van Heuven, S., Hoppema, M., Ishii, M., Jeansson, E., Jones, S. D., Jutterström, S., Karlsen, M. K., Kozyr, A., Lauvset, S. K., Lo Monaco, C., Murata, A., Pérez, F. F., Pfeil, B., Schirnick, C., Steinfeldt, R., Suzuki, T., Telszewski, M., Tilbrook, B., Velo, A., and Wanninkhof, R.:

640   GLODAPv2.2019 – an update of GLODAPv2, Earth System Science Data, 11, 1437–1461, https://doi.org/10.5194/essd-11-1437-2019, https://essd.copernicus.org/articles/11/1437/2019/, 2019.

Orr, J. C.: Recent and future changes in ocean carbonate chemistry, In Ocean Acidification, ed. J-P Gattuso, L Hansson, pp. 41–66, Oxford University Press, Oxford, UK, 2011.

Orr, J. C., Fabry, V. J., Aumont, O., Bopp, L., Doney, S. C., Feely, R. A., Gnanadesikan, A., Gruber, N., Ishida, A., Joos, F., Key, R. M.,

645   Lindsay, K., Maier-Reimer, E., Matear, R., Monfray, P., Mouchet, A., Najjar, R. G., Plattner, G.-K., Rodgers, K. B., Sabine, C. L., Sarmiento, J. L., Schlitzer, R., Slater, R. D., Totterdell, I. J., Weirig, M.-F., Yamanaka, Y., and Yool, A.: Anthropogenic ocean acidification over the twenty-first century and its impact on calcifying organisms, Nature, 437, 681–686, https://doi.org/10.1038/nature04095, https://doi.org/10.1038/nature04095, 2005.

Østerhus, S. and Gammelsrød, T.: The Abyss of the Nordic Seas Is Warming, Journal of Climate, 12, 3297–3304,

650   https://doi.org/10.1175/1520-0442(1999)012<3297:TAOTNS>2.0.CO;2, https://doi.org/10.1175/1520-0442(1999)012<3297:TAOTNS> 2.0.CO;2, 1999.

Perez, F. F., Fontela, M., García-Ibáñez, M. I., Mercier, H., Velo, A., Lherminier, P., Zunino, P., de la Paz, M., Alonso-Pérez, F., Guallart, E. F., and Padin, X. A.: Meridional overturning circulation conveys fast acidification to the deep Atlantic Ocean, Nature, 554, 515–518, https://doi.org/10.1038/nature25493, https://doi.org/10.1038/nature25493, 2018.

655   Raven, J., Caldeira, K., Elderfield, H., Hoegh-Guldberg, O., Liss, P., Riebesell, U., Shepherd, J., Turley, C., and Watson, A.: Ocean acidification due to increasing atmospheric carbon dioxide, Policy document, The Royal Society, London Pp. 1–68, 2005.

Ruiz-Barradas, A., Chafik, L., Nigam, S., and Häkkinen, S.: Recent subsurface North Atlantic cooling trend in context of Atlantic decadal-to-multidecadal variability, Tellus A: Dynamic Meteorology and Oceanography, 70, 1–19, https://doi.org/10.1080/16000870.2018.1481688, https://doi.org/10.1080/16000870.2018.1481688, 2018.

660   Sarmiento, J. L. and Gruber, N.: Ocean Biogeochemical Dynamics, chap. 8, pp. 318–358, Princeton University Press, Princeton, Woodstock, 2006.

Shu, Q., Qiao, F., Song, Z., Zhao, J., and Li, X.: Projected Freshening of the Arctic Ocean in the 21st Century, Journal of Geophysical Research: Oceans, 123, 9232–9244, https://doi.org/10.1029/2018JC014036, https://agupubs.onlinelibrary.wiley.com/doi/abs/10.1029/2018JC014036, 2018.

665   Skjelvan, I., Falck, E., Rey, F., and Kringstad, S. B.: Inorganic carbon time series at Ocean Weather Station M in the Norwegian Sea, Biogeosciences, 5, 549–560, https://doi.org/10.5194/bg-5-549-2008, https://bg.copernicus.org/articles/5/549/2008/, 2008.

Skjelvan, I., Jeansson, E., Chierici, M., Omar, A., Olsen, A., Lauvset, S., and Johannessen, T.: Havforsuring og opptak av antropogent karbon i de Nordiske hav [Ocean acidification and uptake of anthropogenic carbon in the Nordic Seas], 1981-2013. Miljødirektoratet, Rapport M244-2014, Tech. rep., 2014.

670   Skogen, M. D., Hjøllo, S. S., Sandø, A. B., and Tjiputra, J.: Future ecosystem changes in the Northeast Atlantic: a comparison between a global and a regional model system, ICES Journal of Marine Science, 75, 2355–2369, https://doi.org/10.1093/icesjms/fsy088, https://doi.org/10.1093/icesjms/fsy088, 2018.

Somavilla, R., Schauer, U., and Budéus, G.: Increasing amount of Arctic Ocean deep waters in the Greenland Sea, Geophysical Research Letters, 40, 4361–4366, https://doi.org/10.1002/grl.50775, https://agupubs.onlinelibrary.wiley.com/doi/abs/10.1002/grl.50775, 2013.

675 Stöven, T., Tanhua, T., Hoppema, M., and von Appen, W.-J.: Transient tracer distributions in the Fram Strait in 2012 and inferred anthropogenic carbon content and transport, Ocean Science, 12, 319–333, https://doi.org/10.5194/os-12-319-2016, https://os.copernicus.org/articles/12/319/2016/, 2016.

Takahashi, T., Olafsson, J., Goddard, J. G., Chipman, D. W., and Sutherland, S. C.: Seasonal variation of CO_2 and nutrients in the high-latitude surface oceans: A comparative study, Global Biogeochemical Cycles, 7, 843–878, https://doi.org/10.1029/93GB02263, https://agupubs.onlinelibrary.wiley.com/doi/abs/10.1029/93GB02263, 1993.

680

Taylor, K. E., Stouffer, R. J., and Meehl, G. A.: An Overview of CMIP5 and the Experiment Design, Bulletin of the American Meteorological Society, 93, 485–498, https://doi.org/10.1175/BAMS-D-11-00094.1, https://doi.org/10.1175/BAMS-D-11-00094.1, 2012.

Tjiputra, J. F., Assmann, K., and Heinze, C.: Anthropogenic carbon dynamics in the changing ocean, Ocean Science, 6, 605–614, https://doi.org/10.5194/os-6-605-2010, https://os.copernicus.org/articles/6/605/2010/, 2010.

685 Tjiputra, J. F., Roelandt, C., Bentsen, M., Lawrence, D. M., Lorentzen, T., Schwinger, J., Seland, Ø., and Heinze, C.: Evaluation of the carbon cycle components in the Norwegian Earth System Model (NorESM), Geoscientific Model Development, 6, 301–325, https://doi.org/10.5194/gmd-6-301-2013, https://gmd.copernicus.org/articles/6/301/2013/, 2013.

Tjiputra, J. F., Olsen, A., Bopp, L., Lenton, A., Pfeil, B., Roy, T., Segschneider, J., Totterdell, I., and Heinze, C.: Long-term surface pCO_2 trends from observations and models, Tellus B: Chemical and Physical Meteorology, 66, 23 083, https://doi.org/10.3402/tellusb.v66.23083, https://doi.org/10.3402/tellusb.v66.23083, 2014.

690

Turley, C. M., Roberts, J. M., and Guinotte, J. M.: Corals in deep-water: will the unseen hand of ocean acidification destroy cold-water ecosystems?, Coral Reefs, 26, 445–448, https://doi.org/10.1007/s00338-007-0247-5, https://doi.org/10.1007/s00338-007-0247-5, 2007.

Uppström, L. R.: The boron/chlorinity ratio of deep-sea water from the Pacific Ocean, Deep Sea Research and Oceanographic Abstracts, 21, 161 – 162, https://doi.org/https://doi.org/10.1016/0011-7471(74)90074-6, http://www.sciencedirect.com/science/article/pii/0011747174900746, 1974.

695

van Heuven, S., Pierrot, D., Rae, J., Lewis, E., and Wallace, D.: MATLAB Program Developed for CO_2 System Calculations, ORNL/CDIAC-105b. Carbon Dioxide Information Analysis Center, Oak Ridge National Laboratory, US Department of Energy, Oak Ridge, Tennessee., 2011.

van Vuuren, D. P., Stehfest, E., den Elzen, M. G. J., Kram, T., van Vliet, J., Deetman, S., Isaac, M., Klein Goldewijk, K., Hof, A., Mendoza Beltran, A., Oostenrijk, R., and van Ruijven, B.: RCP2.6: exploring the possibility to keep global mean temperature increase below 2°C, Climatic Change, 109, 95, https://doi.org/10.1007/s10584-011-0152-3, https://doi.org/10.1007/s10584-011-0152-3, 2011.

700

Våge, K., Pickart, R. S., Spall, M. A., Moore, G., Valdimarsson, H., Torres, D. J., Erofeeva, S. Y., and Nilsen, J. E. Ø.: Revised circulation scheme north of the Denmark Strait, Deep Sea Research Part I: Oceanographic Research Papers, 79, 20 – 39, https://doi.org/https://doi.org/10.1016/j.dsr.2013.05.007, http://www.sciencedirect.com/science/article/pii/S0967063713001040, 2013.

705 Våge, K., Moore, G., Jónsson, S., and Valdimarsson, H.: Water mass transformation in the Iceland Sea, Deep Sea Research Part I: Oceanographic Research Papers, 101, 98 – 109, https://doi.org/https://doi.org/10.1016/j.dsr.2015.04.001, http://www.sciencedirect.com/science/article/pii/S0967063715000680, 2015.

Zeebe, R. and Wolf-Gladrow, D.: CO_2 in Seawater: Equilibrium, Kinetics, Isotopes, vol. 65 of *Elsevier Oceanography Series*, Elsevier Science, 1 edn., 2001.